CHALMERS
UNIVERSITY OF TECHNOLOGY

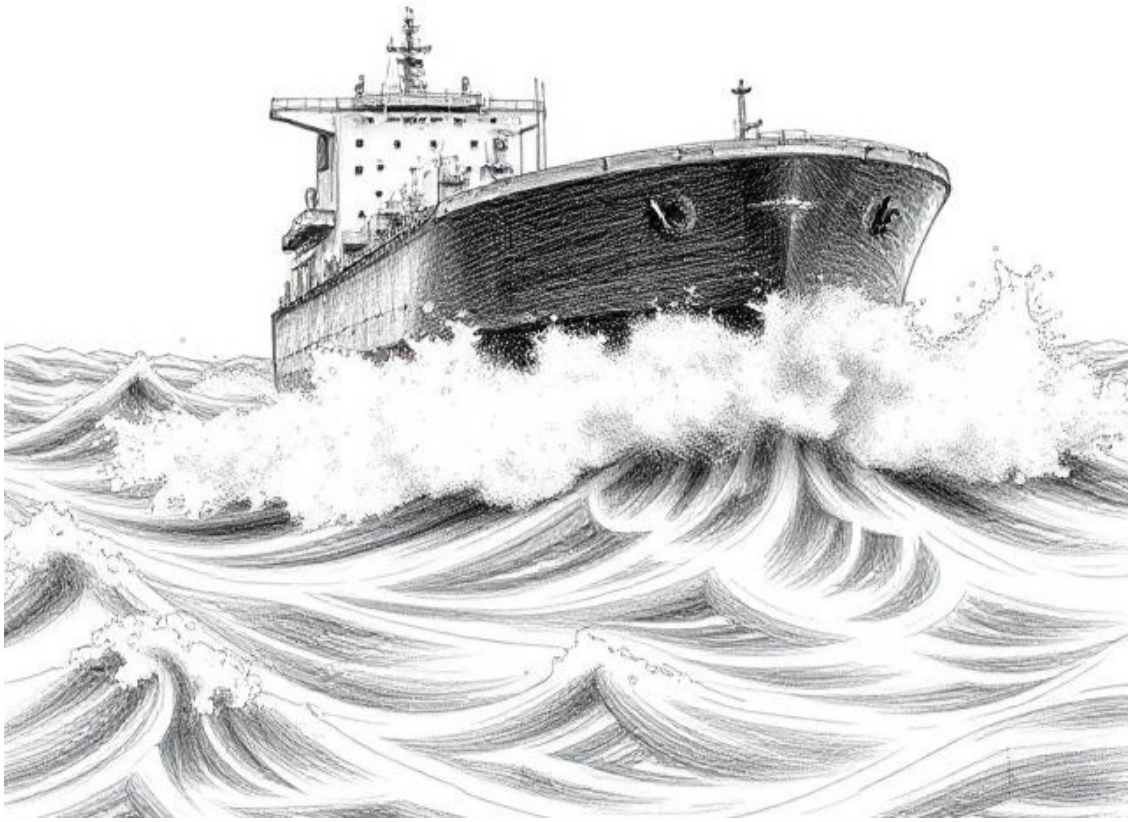

Reducing fuel consumption of tankers in waves

Optimising the main dimensions of next generation MR tankers using Monte Carlo simulations in a performance model

Degree project report in Naval Architecture

Victor Ceder
Nils Helgesson

DEPARTMENT OF MECHANICS AND MARITIME SCIENCES
CHALMERS UNIVERSITY OF TECHNOLOGY
Gothenburg, Sweden 2025
www.chalmers.se

Degree project report 2025

Reducing fuel consumption of tankers in waves

Optimising the main dimensions of next generation MR tankers using Monte Carlo simulations in a performance model

Victor Ceder
Nils Helgesson

CHALMERS
UNIVERSITY OF TECHNOLOGY

Department of Mechanics and Maritime Sciences
Chalmers University of Technology
Gothenburg, Sweden 2025

Reducing fuel consumption of tankers in waves
Optimising the main dimensions of next generation MR tankers using Monte Carlo simulations in a performance model
Victor Ceder
Nils Helgesson

Supervisor: Nicolas Bathfield, Stena Teknik
Examiner: Wengang Mao, Mechanics and Maritime Sciences, Division of Marine Technology

Degree project report 2025
Department of Mechanics and Maritime Sciences
Chalmers University of Technology
SE-412 96 Gothenburg
Sweden
Telephone +46 31 772 1000

Cover: AI generated figure of a tanker in waves using DeepAI.

Typeset in LaTeX
Gothenburg, Sweden 2025

Reducing fuel consumption of tankers in waves
Optimising the main dimensions of next generation MR tankers using Monte Carlo simulations in a performance model
Victor Ceder
Nils Helgesson

Department of Mechanics and Maritime Sciences
Chalmers University of Technology

Abstract

This thesis presents a novel methodology to assess the performance of ocean going commercial vessels. The purpose is to optimise the hull main dimensions in order to reduce the fuel consumption and thus reduce the environmental impact from shipping. This is part of the shipping industry's, through the International Maritime Organisation (IMO), target to reach net-zero greenhouse gas emissions by 2050. The optimisation is Monte Carlo based and the performance of each sample is assessed through a speed loss model based on empirical resistance methods and the SHOPERA-project NTUA NTU MARIC (SNNM) method for added resistance in waves. The environmental factors are extracted from hindcast weather data provided by Copernicus Marine. To improve the accuracy of the predicted added resistance in waves, which is in the order of magnitude of 0-10% of the total resistance, different machine learning models are investigated through processing full-scale measurement data from the IMOIIMAX vessels operated by Stena Bulk, to complement the SNNM model, that is developed and regressed for a broad range of vessel types. In this report, the methodology based on the non-improved SNNM is implemented on, and used to propose main dimensions for Stena's next generation Medium Range (MR) tankers. For the set of weighted routes and weather, the methodology resulted in a design where the model predicted fuel savings of 8.1 % compared to the current generation.

"All models are wrong, but some are useful" - George E.P. Box

Keywords: Added resistance in waves, SNNM, hull optimisation, EEDI, speed loss model, hindcast weather data, machine learning, performance modelling, naval architecture, ship design, ITTC.

Acknowledgements

This report is the result of the Master Thesis carried out together with Stena Teknik. We, Victor and Nils, would like to extend our gratitude to our supervisor Nicolas Bathfield at Stena Teknik for proposing the thesis topic and being a valuable supervisor providing technical and scientific expertise. We would also like to show our appreciation to all colleagues at Stena involved in both the project and chatting around the lunch and fika table.
Stena has welcomed us at their office with open arms and we would like to thank them for all coffee, chocolate, fruit and biscuits that has been consumed by us.
Our examiner Wengang Mao at Chalmers deserves a big thank you for his knowledge within the subject and providing quick and good help when needed.

This study has been conducted using E.U. Copernicus Marine Service Information; https://doi.org/10.24381/cds.bd0915c6, https://doi.org/10.48670/moi-00016.

Victor Ceder & Nils Helgesson, Gothenburg, June 2025

List of Acronyms

CDSAPI Copernicus Data Store API.
CMTAPI Copernicus Marine Toolbox API.

ECMWF European Centre for Medium-Range Weather Forecasts.
EEDI Energy Efficiency Design Index.
ERA5 ECMWF Re-Analysis version 5.

GHG Greenhouse Gas.
GPS Global Positioning System.
GRIB GRIdded Binary or General Regularly-distributed Information in Binary form.

HnM Holtrop and Mennen.

IMO International Maritime Organization.
ISSC International Ship Structures Congress.
ITTC International Towing Tank Conference.

LNG Liquid Natural Gas.
LOA Length Over All.
Lpp Length between Perpendiculars.
LWL Length of Water Line.

MARIN Maritime Research Institute Netherlands.
MR (tanker) Medium Range (tanker).

RoPax Roll-On/Roll-Off Passenger (vessel).

SHOPERA SHip OPERAtions (project).
SNNM SHOPERA-project, NTUA, NTU, MARIC.
SOG Speed Over Ground.
STA-JIP Sea Trial Analysis-Joint Industry Project.
STW Speed Trough Water.

Contents

List of Figures

List of Tables

1

Introduction

This thesis is carried out in collaboration with Stena Teknik to develop a performance model incorporating real weather data. The model is used to optimise the main ship dimensions of next-generation MR tankers, which will help Stena further reduce the fuel consumption of its fleet.

1.1 Background

The International Maritime Organisation is a specialised agency of the United Nations regulating maritime transport. In 2023, IMO member states adopted the new IMO strategy on the reduction of greenhouse gas (GHG) emissions from ships, with the ambition to reach net-zero GHG by 2050 (IMO 2025a). An intermediate goal is to reduce the carbon intensity of international shipping by at least 40% by 2030.

A comparable measure of carbon intensity is the Energy Efficiency Design Index (EEDI), which relates the CO2 emitted to the amount of work (tonne-mile) performed (IMO 2025b). Since 2013, all new ship designs need to achieve an EEDI below a level calculated from ship type and size. This level is to be incrementally tightened every fifth year to continuously reduce the emissions from ships.

The EEDI is calculated with actual data from the sea trials of the newly built ship. More specifically, the speed and power from the Speed/Power Trials. The sea trial serves as the benchmark for the ship and as a receipt that the shipbuilder has delivered a satisfactory ship in accordance to the contract with the shipowner.

The International Towing Tank Conference (ITTC) Recommended Procedures and Guidelines stipulates the technical and environmental conditions for performing Speed/Power Trials (ITTC 2024). One of which is the limiting weather and sea conditions. Normally, all conditions cannot be fulfilled during the actual trials and, therefore, certain corrections have to be made. The experienced sea states affects the resistance of the ship with an additional added resistance in waves R_{AW}, which impacts the achieved speed, power, and therefore also the EEDI of the ship.

Most of the ships design performance is focused on the calm water resistance, without considering the wave environment prevailing on the routes the ship is designed for (Pérez Arribas 2007). Combining the calm water resistance for the ship with

added resistance in waves, a more accurate measure of the ship's resistance while in operations out at sea can be assessed. The hull design with the lowest calm water resistance is not guaranteed to result in the lowest total resistance, including added resistance in waves, R_{AW}.

Stena Bulk operates tankers in different sizes worldwide, some of which are the MR tankers in the IMOIIMAX series. Stena Impero, being one of the 13 ships in this series, is presented in Fig. 1.1. It has the main dimensions shown in Table 1.1.

It is important for Stena to reduce the resistance of their ships since this reduces the power demand for the propulsion system. A lower power demand implies a lower fuel consumption and thus reduced emissions from the operations.

Stena is a company that highly prioritises a minimum environmental impact from its fleet and operations. Stena Teknik, the department responsible for research and development, is interested in exploring what kind of design should be proposed for the next-generation MR (Medium Range) tanker to achieve minimised fuel consumption, with a focus on added resistance in waves.

Figure 1.1: IMOIIMAX vessel Stena Impero

Table 1.1: Main dimensions of Stena's MR tankers in the IMOIIMAX series

Parameter	**Value**
Lpp	179 m
LOA	183 m
B	32.3 m
T	11 m
C_B	0.78
Design speed	14.5 kn
MCR	7211 kW

1.2 Objectives

The objectives of this thesis is to optimise the hull main dimensions of next generation MR tankers, with the IMOIIMAX vessels as a reference. This is achieved by developing a methodology that assesses the energy performance of different designs using hindcast weather data and real trading routes. The focus is on the added resistance in waves through the implementation of the SNNM method. This is complemented by an assessment of whether full-scale data can be used to tune the model to better fit Stena's vessels through machine learning. By varying the main dimensions of the vessel, it will be established which are the most favourable main dimensions from a fuel consumption perspective when taking into account the effect of incoming waves. The methodology is to be used as a decision-supporting tool and as a way of exploring a wide range of design points at Stena.

1.3 Workflow

To achieve to objectives of the thesis, the following tasks will be performed:

- Implement and verify the SNNM method in Python.
- Access and download hindcast weather data from databases.
- Obtain and process full-scale measurement data from reference vessel.
- Implement and evaluate a correction term on the SNNM method.
- Develop a speed loss model for an arbitrary ship.
- Generate samples for Monte Carlo simulations of different hull designs.
- Evaluate the performance of each sample and find optimum.

1.4 Limitations

- The focus is on Medium Range and Suezmax tankers, and a parameter study will not be performed for any other vessel types.
- The implemented method has already been extensively validated by several institutes during development. The model is assumed to be correct, and only verification against available data will be performed.
- No weather routing method will be developed, but the potential implementation will be discussed.
- The thesis will not present any performance data of the Stena vessels. All data presented are "anonymised" and potentially normalised.
- The generated hulls with new main dimensions will only be evaluated for

resistance, thus not evaluated for other criteria such as stability, manoeuvring, etc.

- The thesis does not cover any performance or efficiency enhancing considerations of the propulsion and machinery systems onboard.
- The simulations are run on personal desktop computers, and the size of the Monte Carlo simulations is thus limited to a small sample.

2

Theory

This chapter is a short summary of relevant theory within the field of naval architecture and data technology that is used to develop the methodology and find the optimum hull design. The theory covered includes, but is not limited to, ship resistance, wave theory, propulsive efficiencies and machine learning.

2.1 Ship resistance

A ship is subjected to two main types of forces from the surrounding water, first the hydrostatic force, as a result of the displaced volume of water, denoted buoyancy and acts upwards. When the ship is in motion, hydrodynamic forces acts on the body, the component acting along the axis of movement is denoted as resistance (Larsson and Raven 2010). The dominating component is the calm water resistance, which is what the ship experiences without environmental disturbances such as wind and waves.

2.1.1 Calm water resistance

The ship's calm water resistance is divided into two main components, viscous resistance and wave resistance (Larsson and Raven 2010). The components and their dependencies are presented in Fig. 2.1.

The viscous resistance is commonly divided into four subcomponents: flat plate friction, roughness effects, form effect on friction and form effect on pressure. The wave resistance is divided into wave making and wave breaking resistance (Larsson and Raven 2010).

The flat plate resistance, R_{F0}, is the resistance experienced by running a thin, flat plate through water with equal wetted surface. This is the skin friction giving tangential forces between the solid surface and the water. The skin friction is assumed to be constant when the surface roughness is below a threshold value (Larsson and Raven 2010). This component is severely affected by fouling on the hull.

The hull shape differs from a flat plate, which influences the resistance as well. The 3D shape of the hull increases the resistance and is called the form effect on skin friction. The increased resistance arises due to that the local velocity, compared to

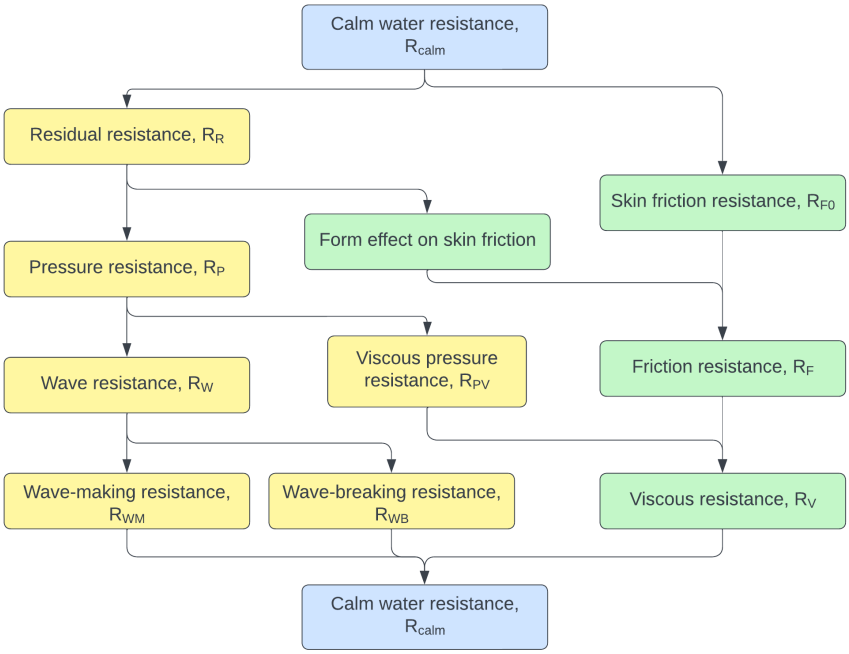

Figure 2.1: Division of ship resistance components and their dependencies.

the free stream velocity of the water, has to increase when going around the hull (Larsson and Raven 2010).

The viscosity of the fluid gives rise to a developing boundary layer along the hull. This will create a difference in pressure between the aftbody and forebody. The pressure at the aft is lower than the fore, and the normal forces due to pressure will increase the resistance of the ship.

The ship's disturbance of the fluid will generate waves, which, if they are steep enough, will break and the energy will dissipate and be found in the wake of the ship. This is called wave breaking resistance. The waves that do not break will radiate away in a Kelvin wave pattern. The energy for this comes from the wave making resistance (Larsson and Raven 2010).

2.1.2 Other types of resistance

In addition to the previously described categories, there are several other types of resistance that, according to Pérez Arribas (2007), can have a significant impact on the ship, such as:

- Induced resistance, a result of gyrations.
- Appendage resistance, from propeller axles, anodes and other appendages.
- Added resistance due to biofouling.
- Added resistance due to the environment.

The effect of the environment is divided into added resistance from winds and added resistance from waves.

This resistance increase is dominated by the added wave resistance, and this effect is traditionally considered by an allowance added to the calm water resistance, denoted sea margin or weather margin. This margin, typically ranging from 15-30% of the calm water resistance, is typically decided from the shipowner or designer's previous experience (Pérez Arribas 2007).

2.1.3 Added resistance in waves

Waves created by wind or swell from other regions can significantly change the resistance experienced by a ship. The resistance increase comes from the induced motion and reflected waves from the seaway. The resistance increase is extra pronounced when the wavelength is equal to or close to the ship length. Both the added resistance in wind and calm water resistance have widely used methods with satisfactory accuracy, such as the Holtrop and Mennen (1982) empirical formula for calm water resistance or obtaining scaled measurements from model tests. Lang and Mao (2021) highlights that the added resistance in waves is still difficult to capture accurately, especially for arbitrary wave heading angles.

Progress of developed models

The first model, developed by Havelock (1942), models the added resistance due to motions, excluding diffraction of waves, viscous damping and coupling between motions. It is limited to head waves only and for wavelengths longer than the ship's length (Pérez Arribas 2007).

Maruo (1957) developed a method based on analytic potential flow calculations with three separate components that are summed up using the superposition principle. The average horizontal force is then calculated and gives the added resistance in waves.

Gerritsma and Beukelman (1972) performed model tests and concluded that the resistance increase for a motionless ship should not be neglected, and that the added resistance is proportional to the wave amplitude squared. The implemented model is based on the radiating energy of the damping waves, using strip theory.

The proposition to divide the components into reflection and induced motion was made by Strom-Tejsen et al. (1973).

Jinkine and Ferdinande (1974) developed a simplified model that could be used to assess added resistance in irregular head seas.

Faltinsen et al. (1980) derived and evaluated an asymptotic formula for the resistance increase of a ship in short waves.

The model developed by Strom-Tejsen et al. (1973) was further improved by Maritime Research Institute Netherlands (MARIN) with the assistance of the Sea Trial

Analysis-Joint Industry Project (STA-JIP) and ITTC as the STAwave-1 (Boom et al. 2019). This method was submitted and included in the ITTC "2012 Guidelines for Speed and Power trials".

STAwave-1 covers only the reflection-induced resistance, R_{AWR}, while the STAwave-2 covers both the resistance increase due to wave reflection, R_{AWR} and the motion-induced resistance, R_{AWM} (ITTC 2014). The STAwave methods are valid for waves from the bow sector ($\pm 45°$) and the ship-specific input is the main dimensions of the ship: L_{pp}, C_B, T_M, B and k_{yy}. They are, however, only valid for long-crested waves.

SNNM

Wang et al. (2021) highlights the challenges and consequences of having these strict limitations since it is common for the conditions at speed trials to be outside the limits of the model.

As a result, the SNNM method was developed within the EU-funded FP7-SHOPERA project (2013-2016) (Liu et al. 2015). The first stages of the project were focused on developing an extended model to be applicable to head-to-beam waves. Using a database of 130 ships and more than 3000 data points, the method was further extended to cover arbitrary wave directions.

The input for the SNNM method is more extensive than the simpler STAwave methods and includes additional parameters such as the angle of entrance and angle of run of the waterline.

The model is restricted to:

- $75 \text{ m} \leq L_{PP} \leq 400 \text{ m}$;
- $5.0 \leq \frac{L_{PP}}{B} \leq 8.0$;
- $2.0 \leq \frac{B}{T} \leq 8.0$;
- $0.52 \leq C_B \leq 0.88$;
- $0.09 \leq Fr \leq 0.30$.

The SNNM was, after its extensive validation, adopted by and included in the ITTC (2021) Preparation, Conduct and Analysis of Speed/Power Trials.

The database the model was regressed for a dataset containing 130 ships consisting of 44.8% Bulker/Gas Carrier/Tanker, 24.1% container and 20.7% Cruise & Roll-On/ROll-Off Passenger vessels (RoPax). The remaining 10.3 % is denoted as "other". With this in mind, the model should have a good fit for a wide range of vessels (Wang et al. 2021).

The Pearson Correlation Coefficient R, when considering all directions, is equal to 0.94 (Wang et al. 2021). This means that the model has a good fit compared to 413

datapoints available for all directions. The added resistance in very short waves is still challenging since the local hull geometry, that cannot be captured by the input parameters, plays a role.

The complete description of the model is appended in Appendix A.

2.1.4 Added resistance due to biofouling

Biofouling is the term used for the involuntary accumulation of plants, algae, microorganisms and animals on submerged or semi-submerged structures. The effects of biofouling are known to increase the resistance of ships. Song et al. (2020) concludes from a wide range of literature that calcareous, hard shell fouling is particularly critical.

According to Woods Hole Oceanographic Institution (1952), the first experimental study on the effect of fouling on frictional resistance was conducted well over 100 years ago by McEntee (1915). Plates with natural barnacles were towed and after 12 months of sea exposure, the resistance when towed saw an increase of 300% compared to the clean plate.

Song et al. (2020) evaluates the penalty of fouling on self-propulsion performance by using CFD, which has the advantage of dynamically computing the local friction velocity distribution for each cell. The study evaluated 10 different surface conditions with either small, medium or big barnacles.

The test case "B20%", with 20% surface coverage of big barnacles, with individual height of 5 mm, yielded an increased total resistance coefficient, C_T, of 52 % for a fouled hull but clean propeller scenario. However, since the hull efficiency and propeller characteristics are affected as well, the propulsive efficiency is reduced, and the shaft power is increased by 57.9 %. The test case, S10% with 10% coverage of small barnacles, resulted in an increased shaft power of 16.3%.

Interestingly, the hull efficiency, η_H, was seen to increase for the fouled hulls, due to increased thrust deduction factor, t and stern wake, w_t.

Other methods to assess the added resistance caused by marine biofouling have been implemented by Turan et al. (2016) which evaluated and towed plates with 3D printed barnacles up to a degree of covering of 5, 10 and 20%. The different barnacle coverages yielded predicted effective power increase of a 280 m Liquid Natural Gas (LNG) carrier travelling at 20 knots at 22.5%, 41.3% and 59.7% respectively.

It can be concluded that, at already a low degree of coverage, the resistance increase is significant when barnacles are present.

Another common type of biofouling is slime coating, a thin but more evenly spread layer of biofilm. The thickness of this microbial film is in the range of millimetres (bacteria) to centimetres (filamentous algae) (Schultz and Swain 2000).

The laboratory-scale drag measurements in Schultz (2007) estimate that the re-

sistance increase for the FFG-7 class frigate of 124 meters and at a speed of 15 knots, with light slime or heavy slime yielded 11% and 21% increase in shaft power, respectively.

The type of fouling and growth rate is a complex mechanism and is dependent on, but not limited to: water temperature, salinity, pH, nutrient abundance, velocity of water flow (ship speed), water depth, light, micro texture, surface charge, wettability, roughness, colours and contours (Uzun et al. 2019).

The model presented by Uzun et al. (2019) managed to predict the increase of resistance due to bio fouling over a three-year period with an accuracy of 4%. The ship studied was a 258 m crude oil carrier operating mainly in the Atlantic ocean.

2.2 Ocean Waves

Regular waves have the shape of a periodic sine wave that moves along the horizontal water surface. The wave surface profile is a function of both time and point (Lewis 1989):

$$\zeta_0 = \zeta \, cos(k_i x - \omega t), \tag{2.1}$$

where:

- ζ Wave amplitude [m],
- k Wave number [-],
- ω wave frequency [rad/s]

Other characteristic measures of a wave are the wave period, T, wave frequency, f and wave length, λ. For deep water, the relations are according to:

$$\omega = \frac{2\pi}{T}, \tag{2.2}$$

$$f = \frac{1}{T}, \tag{2.3}$$

$$k = \frac{2\pi}{\lambda}, \tag{2.4}$$

thus a longer wave will have a lower wave frequency and a higher wave period.

Phase Velocity

The phase velocity, c $[m/s]$, which is the speed of a wave crest, is a direct function of wave frequency and wave number, which in turn is a direct function of wave length (WikiWaves 2025),

$$c \equiv \frac{\omega}{k} = \frac{\lambda}{T}, \tag{2.5}$$

which means a longer wave will be faster than a shorter wave.

The phase velocity is dependent on the water depth. Deep water is valid when the water depth is much greater than the wavelength. Shallow water is defined as when the water depth is much less than the wavelength (WikiWaves 2025).

Group Velocity

The group velocity is the velocity at which a group of waves travels. This is the propagation speed of the wave energy contained in the wave envelope,

$$c_g = c/2 \text{ (Deep water)}, \tag{2.6}$$
$$c_g = c \text{ (Shallow water)}. \tag{2.7}$$

2.2.1 Irregular seas

Waves in the open ocean are characterised by being irregular, thus deviating from the periodic sine wave. The irregular seas can be modelled by the superposition of separate contributions (Krogstad and Arntsen 2000).

$$\zeta_0 = \sum_i \zeta_i(cos(kx - w_i t + \phi_i)) \tag{2.8}$$

where:

- ζ Wave elevation surface,
- ζ_i wave amplitude
- k Wave number [-],
- ω wave frequency.
- ϕ phase shift

Each component has its definite wave frequency and random phase angle. Where the distributions of wave frequency can be described by a frequency spectrum. The most common models are Pierson-Moskowitz, modified Pierson-Moskowitz, Bretschneider, ISSC and JONSWAP. Many of the widely used models are according to ITTC (2002) in the form of:

$$S(w) = \frac{A}{w^5} exp(-B/w^4), \tag{2.9}$$

where:

The parameters used to evaluate the constants A and B differ between models according to Table 2.1

A model-specific constant,
B model-specific exponential constant,
ω wave frequency.

Table 2.1: Definitions of spectral parameters A and B for various wave spectra

Spectrum	***A* and *B* defined in terms of**
One-parameter Pierson-Moskowitz	Significant wave height **or** wind speed or peak period
Two-parameter Pierson-Moskowitz	Significant wave height **and** peak period
ISSC	Significant wave height **and** mean period
ITTC	Significant wave height **and** one of the following: - energy period, - peak period, - mean period, - zero-crossing period

ITTC (2024) stipulates that the modified Pierson-Moscowitz should be used when calculating R_{AW}, with spectrum constants A and B according to Eq. 2.10 and Eq. 2.11.

$$A = 173\frac{H_s^2}{T_{01}^4}, \tag{2.10}$$

$$B = \frac{691}{T_{01}^4}, \tag{2.11}$$

When dealing with irregular waves, wave height is not equal to twice the wave amplitude since the wave height is not constant. A common definition is the significant wave height, which is the average height of the highest one-third of the waves in a given period.

$$H_s = H_{W1/3} \tag{2.12}$$

2.2.2 Short Crested Waves

Waves can be modelled either as short crested or long crested, where ocean waves is characterised by being short crested. Long-crested waves have an elevation that is constant perpendicular to the propagation direction.

The wave components are not only spread in the frequency domain, but also in the directional domain. A commonly used spreading function is the cosine squared. This results in the waves being short-crested, and also dependent on the y-position (Lewis 1989).

ITTC (2024) stipulates that the angular spreading function should be cosine squared when calculating R_{AW}, according to:

$$G(\alpha) = \frac{2^{2s}\Gamma^2(s+1)}{\pi\Gamma(2s+1)}\cos^{2s}(\alpha - \theta_m), \quad \text{for } -\frac{\pi}{2} \leq \alpha - \theta_m \leq \frac{\pi}{2} \tag{2.13}$$

where:

s	Directional spreading parameter,
Γ	Gamma function,
θ_m	Primary wave direction; 0 means heading waves.

The directional spectrum is then the product of the angular distribution function and the frequency spectrum:

$$E(\omega, \alpha) = S_\eta(\omega)G(\alpha) \tag{2.14}$$

where:

G	angular distribution function,
S_η	frequency spectrum.

2.2.3 Global Wave Scatter

Long-term wave statistics have been developed by Hogben (1988), based on measurements dating back to the 1960s. The data includes significant wave height and zero-crossing wave period. This data has then been improved by more recent observations and measurements, but does not include data about the wave spectrum. In the global wave scatter, the oceans are divided into zones, as presented by Fig. 2.2. This has long been the only source for global data.

2.2.4 Wave Forecasting and hindcasting

Since the Second World War's landing operations, the need for predicting the sea state has increased, and a rapid development within this important subject has taken place (Janssen and Bidlot 2018). Wave forecasting is based on the energy balance equation and describes the wave spectrum evolution due to processes driven by wind, non-linear interactions and wave dissipation.

Hindcast models is an approach to simulate past meteorological conditions, such as the wave environment. Hindcast, also known as re-analysis, works the same as

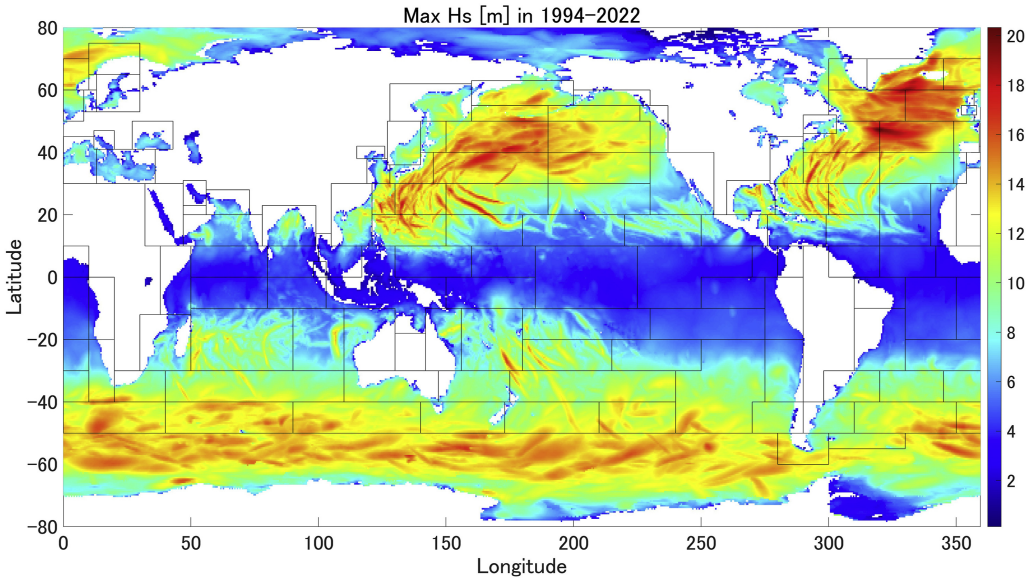

Figure 2.2: The zones used by the global wave statistics plotted together with maximum significant wave height between 1994 and 2022 as approximated by ERA5 (Fujimoto et al. 2024).

forecasting but with a lower resolution in the time domain to allow for datasets spanning longer time periods back in time.

A recent and widely used model is the ECMWF Re-Analysis version 5 model (ERA5), combining the numerical forecast model with available observations to provide an accurate model in a process called data assimilation (Hersbach et al. 2020). The ERA5 model has a spatial resolution of 0.5 ° for ocean waves and a temporal resolution of 1 hour, and a dataset that covers detailed records from 1950 and onwards with a latency of 5 days

2.3 Propulsive efficiencies

The chain from the fuel input to the propulsive force exerted on the ship is long and includes many efficiencies and definitions of variables. In Table 2.2, the different efficiencies and propulsive parameters are defined.

The ship's speed is the speed through water. The arriving water velocity to the propeller is lower than the ship's speed due to the boundary layer, and the water will be decelerated along the hull. The wake fraction coefficient is thus a measure of how much the flow is slowed down compared to the free stream velocity (MAN Energy Solutions 2023).

The propeller suction causes the flow along the hull to be accelerated and thus creates extra resistance. The thrust force, T, exerted by the propeller is thus different to the towing resistance, R_T, (MAN Energy Solutions 2023).

The effective power is the direct function of towing resistance and ship speed, while

the thrust power takes the hull efficiency into consideration. If the wake fraction coefficient, w, is larger than the thrust deduction factor, t, the hull efficiency is greater than one. This is, according to MAN Energy Solutions (2023), usually the case and reduces the power needed to propel the ship.

The propeller efficiency behind the hull, η_B, is the product of the propeller open water efficiency, η_O and the relative rotative efficiency, η_R. With this, the power delivered to the propeller is calculated.

η_O is the propeller efficiency in a homogenous wake field, which is seen when no hull is in front, as tested in a cavitation tunnel. η_R describes the efficiency change due to the flow behind the hull is neither constant nor normal towards the propeller disk's surface (MAN Energy Solutions 2023).

The shaft losses are described by the shaft efficiency, η_S. This is the loss due to shaft bearings and, if installed, the reduction gear. For two-stroke engines with direct coupling, the efficiency is typically around 0.98-0.99, depending on shaft length. and with a reduction gear, around 0.95-0.96 (MAN Energy Solutions 2023).

Table 2.2: Ship propulsion parameters and efficiencies (MAN Energy Solutions 2023)

Velocities	
Ship's speed	V
Arriving water velocity to propeller	V_A
Effective wake velocity	$V_w = V - V_A$
Wake fraction coefficient	$w = \frac{V-V_A}{V}$
Forces	
Towing resistance	R_T
Thrust force	T
Thrust deduction fraction	$F = T - R_T$
Thrust deduction coefficient	$t = \frac{T-R_T}{T}$
Power	
Effective (Towing) power	$P_E = R_T V$
Thrust power delivered by the propeller to water	$P_T = \frac{P_E}{\eta_H}$
Power delivered to propeller	$P_D = \frac{P_T}{\eta_B}$
Brake power of main engine	$P_B = \frac{P_D}{\eta_S}$
Efficiencies	
Hull efficiency	$\eta_H = \frac{1-t}{1-w}$
Propeller efficiency - open water	η_O
Relative rotative efficiency	η_R
Shaft efficiency	η_S
Engine efficiency	η_E
Propeller efficiency - behind hull	$\eta_B = \eta_O \eta_R$
Propulsive efficiency	$\eta_D = \eta_H \eta_B$
Total propulsive efficiency	$\eta_{\text{prop}} = \eta_H \eta_B \eta_S$
Total efficiency	$\eta_{\text{tot}} = \eta_{\text{prop}} \eta_E = \eta_H \eta_O \eta_R \eta_S \eta_E$

2.4 Speed loss prediction models

The speed loss ΔV is the difference between the ship speed in ideal sailing conditions V_{calm} and the experienced speed V_{real} (Pérez Arribas 2007).

$$\Delta V = V_{calm} - V_{real} \tag{2.15}$$

A speed loss prediction model is used to predict the involuntary speed losses caused by weather and wind. This is different from the voluntary speed losses due to operating decisions that are taken in order to save fuel or due to navigation and manoeuvring reasons.

A proper speed loss model needs to be able to model the engine and propeller characteristics for different operating scenarios. It also needs a reliable method of predicting the total resistance including calm water resistance, added resistance in waves and wind.

2.5 Machine learning and regression of formulae

Regression with one response variable is called univariate regression, while models with two or more response variables is called multivariate regression (Chatterjee and Hadi 2012).

Predictor variables can be seen as the input of which is assumed to influence the output, commonly denoted the response. The amount of predictor variables defines if it is a univariate or multiple regression. With two or more predictor variables, we have multiple regression.

Regression can be either linear or non-linear, where non-linear is more complex and computationally demanding. For a linear regression, all predictor variables enter the equation linearly or can be transformed to a linear format (Chatterjee and Hadi 2012). Eq. 2.16 show a simple linear equation, Eq. 2.17 shows a linearisable function and the linearisation, Eq. 2.18. An example of a non-linear function that cannot be transformed is shown by Eq. 2.19.

$$Y = \beta_0 + \beta_1 X + \beta_2 X + \varepsilon \tag{2.16}$$

$$Y = \beta_0 + \beta_1 lnX + \beta_2 X^2 + \varepsilon \tag{2.17}$$

$$(X_1 = lnX,\ X_2 = X^2) \Rightarrow Y = \beta_0 + \beta_1 X_1 + \beta_2 X_2 + \varepsilon \tag{2.18}$$

$$Y = \beta_0 + exp(\beta_1 X) + \varepsilon \tag{2.19}$$

Regression is performed on available data to estimate the parameters β_i such that as good a fit as possible is achieved. A common method is *least squares*, which minimises the sum of squared errors between the model and data.

$$S(\beta_0, \beta_1, ..., \beta_n) = \sum_i \varepsilon_i^2 \tag{2.20}$$

There are two main categories of ML models: whitebox and blackbox. A white box model is a model where the logic is transparent and easy to interpret; it is clear to see how each parameter influences the prediction of the model. Black box models are more complex and often offer no transparency at all. A black box model is usually more accurate, especially for complex nonlinear problems. However, because of its non-transparency, it may behave unexpectedly on data that is not in the training set, and debugging and determining how each input affects the output can be more difficult can be done using additional tools. A white box model has the advantage of being predictable and more stable for the extrapolation of new inputs not in its training data. A white box model might be preferred when explainability and transparency of the logic are more important than the accuracy of the predictions. Some common models are explained below (Lang et al. 2022).

Linear regression

Linear regression is a simple white box model; it takes input and tries to find two parameter values, k and m, to fit y=kx +m as explained above, Eq. 2.16 to Eq. 2.18. Every input is then interpreted in a linear function and summed together create the prediction (Olive 2017).

Random Forest

Random forest model is a blackbox model based on decision trees, typically used for classification problems. However, in a random forest, many trees are used and averaged, and this model can be used in this thesis as a regression model. These "forests" grow large, and it is technically possible to see how each tree is built; it is not practically feasible (Breiman 2001).

XGBoost

XGBoost (Extreme Gradient Boosting) is an ensemble model based on random forest but incorporates boosting. Boosting means that models are built on previous models, in this case, decision trees, which give faster results and allow each tree to correct errors in the previous tree. The model also incorporates measures to reduce overfitting, which can be a problem with the random forest method (Chen and Guestrin 2016).

3

Methods

In order to achieve the objectives of this thesis, a systematic methodology consisting of a network of methods has been used. Some are developed by the authors, while others are implementation of well known and widely used methods. This chapter presents the framework for these methods. Fig. 3.1 illustrates how the different methodologies connect and how the optimised hull depends on many methods to be evaluated. The lower left branch containing measured data serves the purpose of validating the SNNM towards full scale measurements, and also to improve the model using machine learning. The lower right leg is where the optimisation and evaluation are performed. This leg can be independent of the left one by using the standard SNNM model.

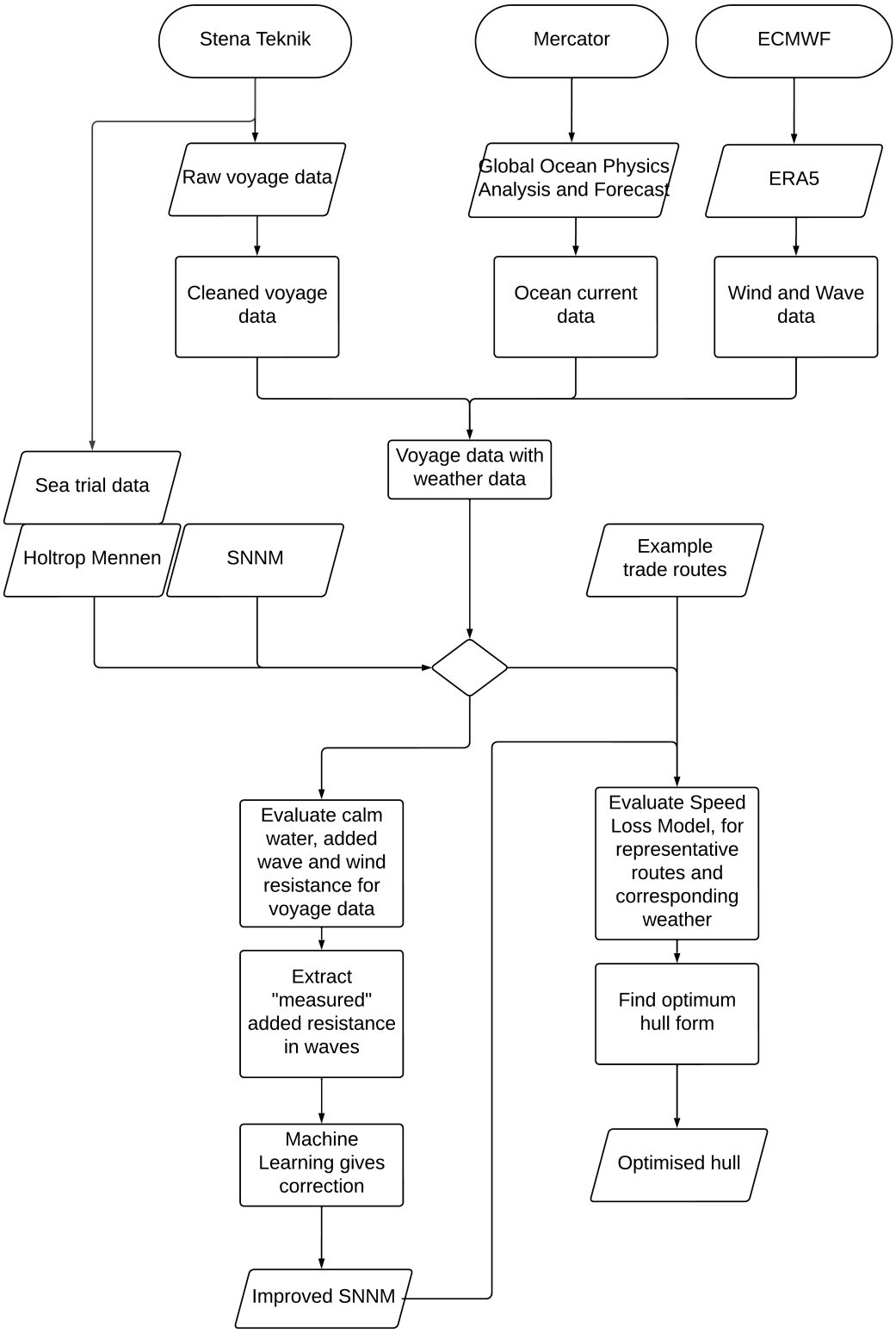

Figure 3.1: Flowchart describing the overall method.

3.1 SNNM

The SNNM method published in ITTC (2024) has been implemented in a Python script. Calculations of added resistance are following ITTC procedures. The SNNM method has been intensively validated for a broad range of ships and has proven to predict the added resistance with satisfactory accuracy over the studied range of vessels and wave environments.

The method is complex and includes several parts that are open to interpretation; see Section 3.1.1. In order to verify that the SNNM is implemented correctly, the results for a benchmark ship have been compared to the results provided by MARIN. The MARIN results are based on (Liu and Papanikolaou 2020), which differs from what is published in ITTC (2024). The differences and inconsistencies between the different versions are explained in more detail in Section 3.1.1. The latest version as published in ITTC (2022) and ITTC (2024) is found in Appendix A.

3.1.1 Inconsistencies

In the guidelines of ITTC (2024), the SNNM method is referenced to Liu et al. (2015) which does not present the SNNM equations in a consistent format. Liu and Papanikolaou (2016) presents the equations more thoroughly but is still not consistent with ITTC (2024). The formulae and coefficients for the SNNM method were improved in Liu and Papanikolaou (2020), which starts to resemble the present formulae.

ITTC 2021 was the first inclusion of SNNM in 7.5-04-01-01.1: Procedure Preparation, Conduct and Analysis of Speed/Power trials, which, compared to the Liu and Papanikolaou 2020 method, has other formulas for a_2, with a separate function for following seas and interpolation in between. The interpolation for stern oblique waves is performed on the constants a_1 and a_2.

ITTC 2022 updated the SNNM calculations with modified formulae. In this revision, the condition for the a_2 constant changes from $V_s \leq V_g/2$ to $V_s \leq V_g$ and the interpolation for stern oblique seas is now made for R_{AWM} instead of a_1 and a_2. Due to R_{AWM} not being a linear function of a_1 and a_2, this will not produce the same results.

The most recent revision of 7.5-04-01-01.1 ITTC (2024) has equations and procedures regarding SNNM and added resistance in line with the previous revision ITTC (2022).

3.1.2 Directional spectrum

The directional spectrum describes the distribution of short-crested irregular waves concerning frequency and directional domain according to Section 2.2, where ITTC (2024) stipulates that the directional spectrum should use modified Pierson-Moscowitz in the frequency domain and cosine squared according to Eq. 2.13, in the directional

domain. The influence of the parameters on the directional domain is visualised in Fig. 3.2 where a baseline is defined in a). This baseline represents common wave conditions found in Section 4.1.1 and following waves. Even though the main wave direction is $180° = \pi\ rad$, a significant amount of wave components with direction other than pure following is also present.

In b), the change from s=1 for wind waves to s=75 for swells significantly changes the directional spreading to be more concentrated around the primary wave direction.

In c) the primary wave direction is changed to 45°, which shifts the wave components to be centred around quartering waves. Note that the width of the directional spectrum results in some wave components coming in from angles on the other side of head waves (0°).

For this thesis, the directional spreading s=75 for swells is used as this is representative for the environment prevailing on the open ocean.

3.1.3 Convergence study

For assessing the added resistance in short-crested irregular waves, a double integral has to be computed by Eq. 3.1.

$$R_{AW} = 2\int_0^{2\pi}\int_0^{\infty} \frac{R_{wave}(\omega,\alpha;V_s)}{\zeta_A^2} E(\omega,\alpha)\, d\omega d\alpha \tag{3.1}$$

where:

R_{wave}	Transfer function, mean resistance increase
ω	Wave frequency,
α	Wave encounter angle
V_s	Ship speed
ζ_A	Wave amplitude
$E(\omega,\alpha)$	Directional wave spectrum

The integral is calculated using a trapezoid method with discretisation of the spectrum from 0 to 2π in α direction. R_{wave} is the transfer function of the mean resistance increase in regular waves. The directional wave spectrum is influenced by T_p, α, and the directional spreading factor, s. It is thus only necessary to integrate over a domain where the directional spectrum has a significant value. Since the integrand is diverging at $\omega = 0$, the lower limit is set to 0.01 in the ω direction. As integrating to infinity in the ω direction is not feasible, the upper limit of $\omega = 6$ is used.

The upper limit of the wave frequency, $omega = 6$, is equal to waves with a wavelength of 1.7 meters and a wave period, $T = 1.05\ s$, which can be seen in Section 4.1.1 to be a suitable lower limit on wave period.

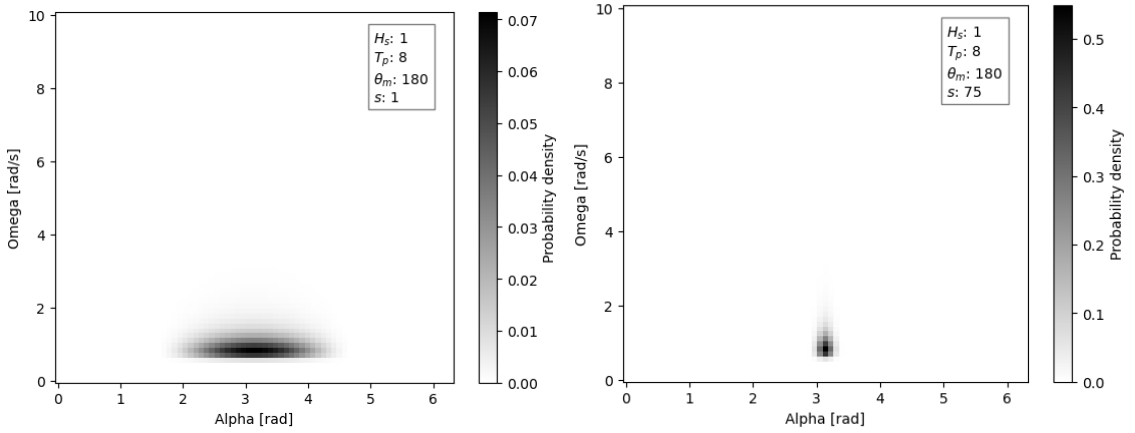

(a) Baseline.

(b) Changed to spreading parameter for swells.

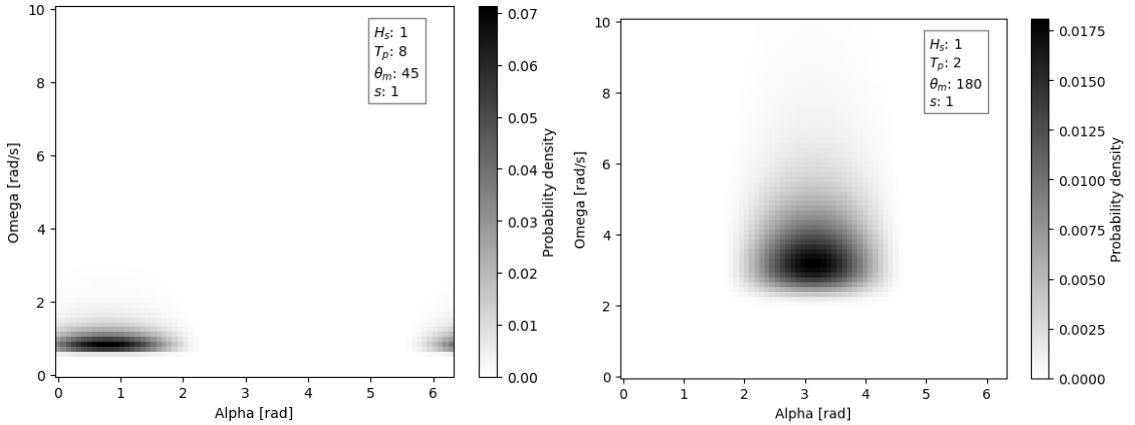

(c) Changed primary wave direction to quartering waves.

(d) Changed to lower peak time period, T_p.

Figure 3.2: Variation of individual parameters for wave directional spectrum and corresponding results.

The lower limit of the wave frequency, $\omega = 0.01$, is equal to a wavelength of 617 km and a wave period of $T = 628\ s$. The consequences of choosing to include these long wavelengths are assessed in Section 7.3.

The resolution (number of discretisation points) highly influences the calculation time. To select and motivate a satisfactory but computationally quick grid, a convergence study is performed for quadratic grid sizes, XxX, from 10x10 to 200x200 points, X number of points on the span $[0 < \alpha < 2\pi]$ and X number of points on the span $[0.01 < \omega < 6]$. The ship parameters used for the convergence study are from the IMOIIMAX series from Stena Bulk. The selection of wave conditions is made for the most encountered combination of $H_s = 1.5\ m$ and $T_p = 8\ s$. The speed is set to 13 knots. See Section 4.1.1 for reference.

Fig. 3.3 shows the added resistance as calculated by SNNM method for head, beam,

stern oblique and following waves for the specified range. It is seen that, for this combination, the values converges at a grid resolution of 50x50 points. The convergence might be reached at higher resolutions for other combinations of waves and speed. Therefore, the resolution is set at 75x75 to ensure satisfactory results while still maintaining efficient calculation times. The computation time, as a function of grid resolution, is presented in Fig. 3.4. With the desktop computer setup used in this project, a grid of 50x50 points results in a calculation time of 0.2 seconds for the wave making resistance in one time instance, and a 200x200 grid results in 3.3 seconds, an increase by a factor of 16. The computational time seems, as expected, to increase quadratically with the number of points in each direction since the total number of points is the square of that.

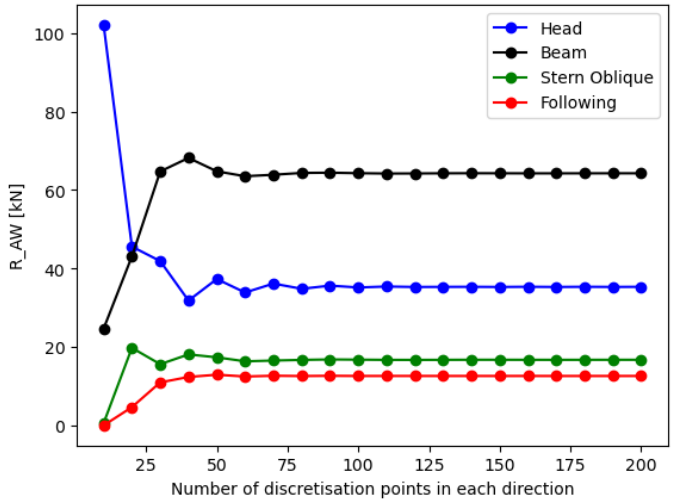

Figure 3.3: Convergence study for added resistance on different grid resolutions for head, beam, stern oblique and following waves.

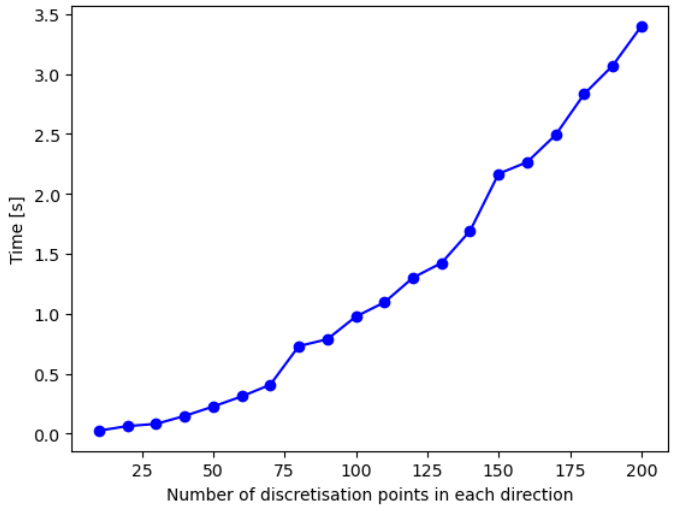

Figure 3.4: Computational times for different grid resolutions in the convergence study.

3.2 Retrieving marine and oceanographic data

The data used in this project is retrieved from Copernicus. The wave and wind data is given by the ERA5 (Hersbach et al. 2020) dataset available at Climate Data Store (2025). The ocean currents are accessed from the Global Ocean Physics Analysis and Forecast (Copernicus Marine Services 2025b) available through Copernicus Marine Services (2025a).

The data is accessed trough Climate Data Store API (CDSAPI) and Copernicus Marine Toolbox API (CMTAPI) respectively. The wave and wind data from the ERA5 dataset, described in Section 2.2.4, is accessed trough CDSAPI in a Gridded Binary (GRIB) format, which is a heavily compressed format which is quick to download and allocates less disk space. The current data is accessed via the CMTAPI and is downloaded as a ZARR-format (Miles et al. 2025), which is also a compressed format but is larger than the GRIB format.

Copernicus Marine Service

Copernicus Marine Services (2025a) provides free, regular and systematic authoritative information. The service is implemented by Mercator Ocean International, funded by the European Commission to boost the Blue Economy within the maritime industry.

This study has been conducted using E.U. Copernicus Marine Service Information (Copernicus Marine Services 2025b). Results from this thesis are generated using Copernicus Climate Change Service information (Climate Data Store 2025).

Climate data store

The Climate Data Store (2025) is the modernised version of Copernicus Marine Services (2025a). This is implemented by the European Centre for Medium-Range Weather Forecasts (ECMWF) and run on their Common Cloud Infrastructure (CCI).

3.3 Measured voyage data and analysis

In order to tune the SNNM model to have a more accurate prediction of R_{AW}, the introduction of full scale measurement data is introduced. The measure data will in combination with weather data from Copernicus, be used to extract the added resistance in waves.

Stena's IMOIIMAX series measure, process and store data from the operations. The voyage data is given in CSV format, with 89 columns of unique variables, some of which are calculated from other measured variables. The variables used in this thesis are listed in Table 3.1 below. The data consists of hourly averages from 2024-06-24 until 2025-02-25 covering the Atlantic ocean, Indian ocean and some of the north sea. The track covered is presented in Fig. 3.5. It is possible to extract data with much higher temporal resolution than one hour, but due to the limitations regarding

Table 3.1: Voyage measurements used in the project

Parameter	**Unit**
Sensor Hour	timestamp
Latitude	degrees
Longitude	degrees
Ship Course	degrees
Main Engine Shaft Torque	kNm
Main Engine Shaft Speed	RPM
Ship Speed GPS	kn
Ship Speed Log	kn
Draft Aft	m
Draft Forward	m
Draft Mean	m
Wind Direction Absolute	degrees
Wind Direction Relative	degrees
Wind Speed Absolute	kn
Wind Speed Relative	kn

computational power, it is preferred to have lower resolution but for a larger set of operational conditions, i.e., longer date extent of the data.

The data represent the ship's typical operations. With real voyages and actual times and speeds. The ship track is mapped to the hindcast weather data, further explained in Section 3.3.2.

Using the delivered power and calculating backwards, the "measured" resistance can be extracted. The calm water resistance can also be approximated using known resistance curves or formulas. The difference between calm water resistance and the measured resistance is assumed to be the added resistance. The difference between predicted and measured added resistance is denoted ε. Machine learning will be used to introduce a model for the correction that reduces this difference, i.e closing the gap.

3.3.1 Preprocessing voyage data

The data needs to be processed, the first criteria to be filtered out is if Global Positioning System (GPS) position is missing. Here, missing is treated as equal to 0. The coordinate 0,0 exists outside the coast of Africa, commonly called the Null-Island by the geospatial community (Wikipedia 2025), but the probability of having the exact location 0,0 is extremely close to zero since the GPS data has so many significant digits that the accuracy is in the magnitude of centimetres.

The data is then cleaned by filtering out all measurement points with Speed oVer Ground (SOG) <11 kn and Speed Trhough Water (STW) <11 kn. This is to remove data points from when the ship is in port or slowly approaching port, and to only include data where there is speed trial data for the resistance.

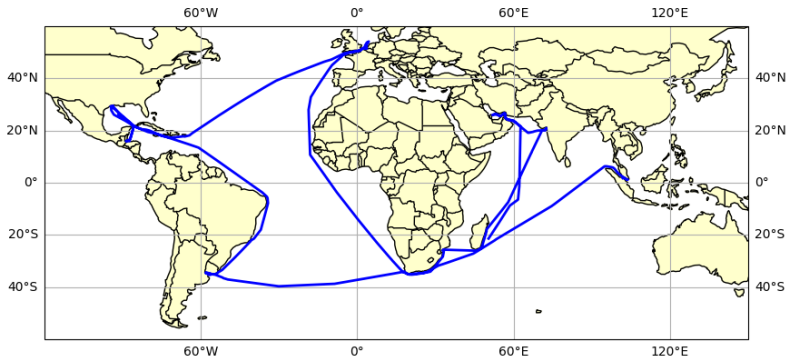

Figure 3.5: Traversed voyages included in the dataset, spanning from 2024-06-24 until 2025-02-25

Additionally, some GPS anomalies are present in the data. To consider this, all data points that have an unreasonable distance to next data point, here above 40 km, equal to the distance travelled over 1 hour at 35 knots, are filtered out.

For each filter, the number of data points removed is stored and presented to indicate the quality and usability of the data.

3.3.2 Mapping hindcast weather data to voyage data

The GPS track supplies the information of when and where the ship is located. The ERA5 re-analysis gives global data for a given time, with a resolution of 1 hour. The voyage data needs to be mapped to extract the ERA5 data at the correct location and time for each time instance. This is handled in Python by extracting the closest position with weather data to the GPS position. No interpolation of values is thus used.

3.3.3 Extracting added resistance in waves from full scale measurement data

As previously described, the measured added resistance in waves is extracted through the delivered power and calculating backwards to achieve the measured resistance and comparing it to the predicted calm water resistance. The measurement data provides measured delivered power, P_D which is converted into total resistance, R_T by:

$$R_T = \frac{T_S \cdot N_S \cdot \frac{\pi}{60} \cdot \eta_S \cdot \eta_D}{V_K \cdot \frac{1852}{3600}}, \tag{3.2}$$

where:

T_S	Shaft Torque [kNm],
N_S	Shaft Speed [rpm],
V_K	Ship speed [Kn],
η_S	Shaft efficiency [-],
η_D	Propulsion efficiency[-].

The goal is both to extract the added resistance in waves in order to validate the implemented SNNM model and also use machine learning to develop a ship specific model with a better fit of the results.

In order to extract the added resistance in waves, the other components need to be identified and approximated, and relevant environmental effects need to be considered.

The total resistance is the sum of calm water resistance, air resistance, and added resistance in waves, as described by ITTC (2024):

$$R_T = R_{calm} + R_{AA} + R_{AW}(+R_{AS}), \tag{3.3}$$

where:

R_T	Total resistance,
R_{calm}	Calm water resistance,
R_{AA}	Added air resistance,
R_{AW}	Added resitance in waves,
R_{AS}	Added resistance due to deviation of water temperature and density, this is neglected in this project.

Calm water resistance

The calm water resistance is the dominating component, which can be approximated in a number of ways. For the estimation of calm water resistance, three methods are evaluated:

- Empirical resistance method (Holtrop and Mennen 1982)
- Scaled model test data
- Speed trial data

The empirical resistance method of Holtrop-Mennen is widely used and serves as a good approximation. For the current vessel, both model test data and speed trial data are available. The calm water resistance curves can be seen, though anonymised, in Fig. 3.6. Holtrop and Mennen overstimates the resistance by 9.7% on average and the towing tank test prediction was on average 6.4% lower than the speed trial test.

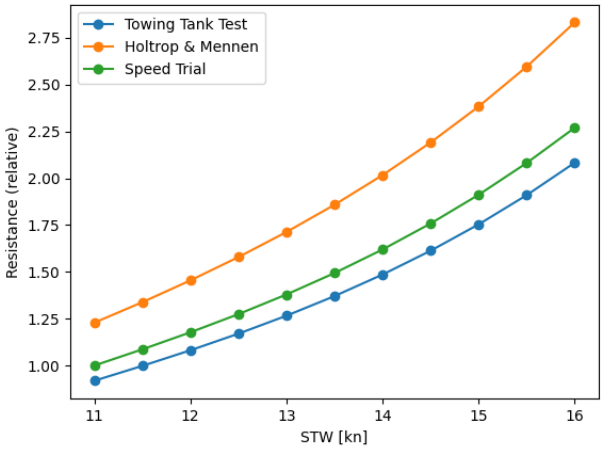

Figure 3.6: Show the discrepancies between the towing tank test, speed trial test and approximation method by Holtrop and Mennen (1982), at design draft of 11 m.

The speed trial data is assumed to be the most correct and is used in combination with the recorded ship data to extract the added resistance in waves.

Since the measured data include both ballast and laden conditions, but model tests are only performed for ballast, design and scantling draft, the effect of draft changes needs to be considered. In other words, a two-dimensional resistance curve is needed, since the resistance is given by both the speed and the draft. The resistance as a function of draft is illustrated in Fig. 3.7 below. Note that the speed trial only has values at 7.25 m, 11 m and 12.9 m, in between these points, linear interpolation is used. The values outside of this range is assumed to be constant with the values at the end points (7.25 m and 12.9 m). The ship would not reach a draft above scantling (12.9 m) or below ballast (7.25 m) under normal conditions.

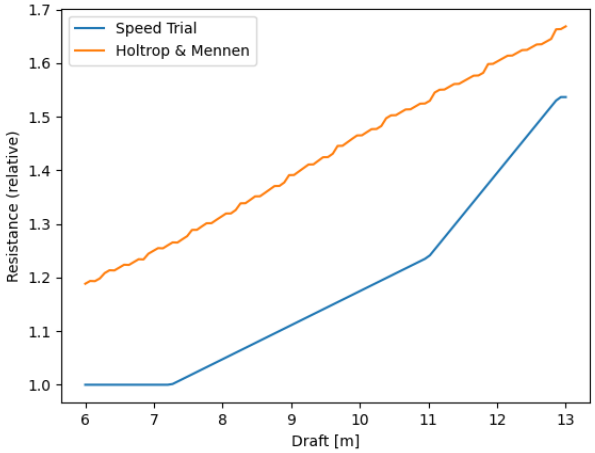

Figure 3.7: Resistance as a function of draft for a constant speed of 12 knots, here speed trial data and Holtrop and Mennen is compared.

Effect of ocean currents

The ship's STW and SOG are often found to differ. This is due to the effect of ocean currents. Ideally, the ships' measured STW can be used as input to the SNNM and speed loss model. However, this measurement can differ from reality, both due to calibration and measurement errors, since the transducer is measuring within the boundary layer and does not capture the free stream velocity.

An alternative method of approximating the STW is made using SOG combined with prevailing currents.

The ERA5 hindcast data does not provide ocean currents, but it can be accessed through other datasets such as the Mercator global ocean analysis and forecast, which provides hourly data at a spatial resolution of 1/12°.

The ship's STW can then be approximated using the SOG, course, current and its direction, by employing vector algebra:

$$\mathbf{V}_{SOG} = SOG \cdot (\cos(\theta_{COG}), \sin(\theta_{COG})), \tag{3.4}$$

$$\mathbf{V}_{current} = V_{current} \cdot (\cos(\theta_{current}), \sin(\theta_{current})), \tag{3.5}$$

$$\mathbf{V}_{STW} = \mathbf{V}_{SOG} - \mathbf{V}_{current}, \tag{3.6}$$

$$V_{STW,x} = SOG \cos\theta_{COG} - V_{current} \cos\theta_{current}, \tag{3.7}$$

$$V_{STW,y} = SOG \sin\theta_{COG} - V_{current} \sin\theta_{current}, \tag{3.8}$$

$$STW = \sqrt{V_{STW,x}^2 + V_{STW,y}^2}, \tag{3.9}$$

$$\theta_{STW} = \tan^{-1}\left(\frac{V_{STW,y}}{V_{STW,x}}\right), \tag{3.10}$$

where:

SOG	Ship speed over ground [m/s],
$\mathbf{V}_{SOG}$	Vector of SOG with components in latitudinal and longitudinal direction,
θ_{COG}	Ship course over ground [deg],
$V_{current}$	Absolute velocity of current [m/s],
$\mathbf{V}_{current}$	Vector of current velocity with components in latitudinal and longitudinal direction,
$\theta_{current}$	Absolute angle of the current [deg]
STW	Speed through water [m/s]
$\mathbf{V}_{STW}$	Vector of STW with components in latitudinal and longitudinal direction,
θ_{STW}	Absolute angle of STW

Effect of wind resistance

The added resistance due to wind is evaluated using experimental resistance coefficients from F.3 in ITTC (2024) presented in Table 3.2. The table features positive values for wind angles behind midship. This implies that the wind propels the ship forward. The provided data is for a 280 kDW tanker with a conventional bow, where a profile view is presented in Fig. 3.8. The added resistance due to wind is calculated from the Apparent Wind Speed and Direction (AWS and AWD). This is also obtained using vector algebra according to Eq. 3.11 to Eq. 3.15.

Table 3.2: Cx coefficients vs. Angle of Attack for Ballast and Laden conditions

Angle of attack [deg]	**Cx Ballast [-]**	**Cx Laden [-]**
0	-0.86	-0.96
10	-0.76	-0.93
20	-0.62	-0.85
30	-0.45	-0.73
40	-0.32	-0.62
50	-0.21	-0.47
60	-0.13	-0.34
70	-0.06	-0.17
80	-0.04	-0.06
90	0.02	0.05
100	0.08	0.14
110	0.19	0.22
120	0.29	0.29
130	0.38	0.40
140	0.47	0.53
150	0.56	0.66
160	0.61	0.75
170	0.66	0.79
180	0.61	0.75

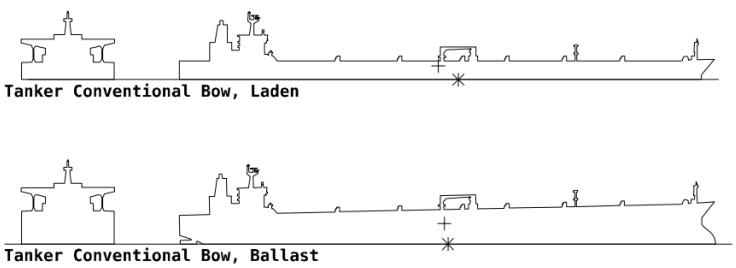

Figure 3.8: Profile view of 280 kDW tanker corresponding to C_X data (ITTC 2024).

$$\text{TWD} = (\text{WD} - \text{Ship Course}) \bmod 360, \tag{3.11}$$

$$U = V_s + \text{WS} \cdot \cos\left(\frac{\pi}{180} \cdot \text{TWD}\right), \tag{3.12}$$

$$V = \text{WS} \cdot \sin\left(\frac{\pi}{180} \cdot \text{TWD}\right), \tag{3.13}$$

$$\text{AWS} = \sqrt{U^2 + V^2}, \tag{3.14}$$

$$\text{AWD} = \left(\frac{180}{\pi} \cdot \arctan 2(V, U)\right) \bmod 360, \tag{3.15}$$

where:

WD	Wind direction [deg],
WS	Wind speed [m/s],
TWD	True wind direction [deg],
V_s	Ship speed [kn],
AWS	Apparent wind speed,
AWD	Apparent wind direction.

The added resistance due to wind, R_{AA} is then calculated through:

$$R_{AA} = -\frac{1}{2} C_X \rho_a A_{xv} V_{rel}^2, \tag{3.16}$$

where:

R_{AA}	Added resistance due to wind [N],l
C_X	Drag coefficient [-],
ρ_a	Density of air [kg/m^3],
A_{xv}	Frontal wind area of ship,
V_{rel}	Relative speed between wind and ship.

Biofouling resistance

As explained in Section 2.1.4, modelling the resistance increase from biofouling is a complex problem and out of scope for this project.

The models also need information on the time of cleaning, which is not available. Additionally, more parameters need to be extracted from the ERA5 dataset and potentially from other sources as well. This will significantly increase the complexity of the model and the computational time.

3.3.4 Assumptions

- Induced resistance is assumed to be zero. See Section 2.1.2.
- Added resistance due to biofouling is not considered

- Linear interpolation of the resistance curves with regards to draft is assumed to be reasonably valid, i.e., peaks or troughs of the resistance in-between ballast, design and scantling draft are not considered.
- STW reading from ship data is correct
- Deviation of water temperature and density neglected

3.4 Improved SNNM

A machine learning model is used to close the gap between the SNNM estimation of the added resistance in waves and the added resistance in waves extracted from full-scale measurement data.

The error term, ε, is introduced as:

$$\varepsilon = R_{AW,measured} - R_{AW,SNNM}, \tag{3.17}$$

where:

$R_{AW,measured}$	R_{AW}s extracted from measurements,
$R_{AW,SNNM}$	R_{AW} with the SNNM method

The machine learning model has the purpose of approximating this error such that it can be used as a correction term, increasing the accuracy of the predicted added resistance in waves.

$$R_{AW}^{improved} = R_{AW}^{SNNM} + \varepsilon_{ML}(x_1, x_2, ..., x_n) \tag{3.18}$$

where:

$R_{AW}^{improved}$	Improved prediction of R_{AW},
$R_{AW,SNNM}$	R_{AW} calculated with the SNNM method,
$\varepsilon_{ML}(x_1, x_2, ..., x_n)$	Machine learning model based on parameters 1 to n.

3.4.1 Choice of machine learning algorithms

Lang et al. (2022) makes a comparison of several typical supervised machine learning algorithms: extreme gradient boosting (XGBoost), artificial neural network, support vector machine, and statistical regression methods. The article utilises metocean data as well as full-scale measurement data from two ships. The article concludes that XGBoost achieved much better predictions than statistical regression models. Even compared to more complex artificial neural networks and support

vector regression, XGBoost was determined to be slightly better and required less training time. This information is valuable for this thesis project, since the goal and dataset are similar. Based on this previous paper, a few models are compared: random forest regression, XGBoost and linear regression.

3.4.2 Training the model

The voyage data is split into a training set of 80% and a test set of 20%, which allows checking the predictions of the model on new data points that were not used in the training.

Random search for hyperparameters will be applied to the Random Forest Model and XGBoost model, which will improve the performance of the models and avoid setting bad hyperparameters. The Linear Regression model will be treated differently. It is known that this problem is not linear; to increase the accuracy of this model, the input parameters are modified. Table 3.3 shows the input parameters for the models. For the linear model, the ship velocity is modified to V^2, in MAN Energy Solutions (2023), it is explained that the resistance is proportional to the velocity squared, based on Bernoulli's equation on dynamic pressure.

Table 3.3: Voyage parameters for regression models

Parameter	**Linear**	**Random Forest**	**XGBoost**
Mean Draft [m]	x	x	x
STW [kn]		x	x
STW^2 [kn^2]	x		
Hs [m]	x	x	x
Tp [s]	x	x	x
Relative Wave Direction [rad] (0-π)		x	x
sin(Relative Wave Direction [rad])	x		
cos(Relative Wave Direction [rad])	x		

The Random Forest model and XGBoost can adapt to non linear problems. However, some parameters are adapted to better model the non-linearites of the problem for input into the linear regression model.

The hyperparameters, the settings of the model, are set by employing a randomised search. Reasonable intervals for each hyperparameter are given manually, and different combinations are generated randomly and evaluated. This is faster than a more thorough search, checking each combination of hyperparameters. The hyperparameters with the best performance are then used. This reduces manual testing and makes sure that good hyperparameters are selected.

The hyperparemeters used for random forest are listed in Table 3.4 and for XGBoost in Table 3.5.

Table 3.4: Chosen hyperparameters for random forest model, hyperparameters not listed are kept as default

max_depth	20
max_features	log2
min_samples_leaf	2
min_samples_split	2
n_estimators	200

Table 3.5: Chosen hyperparameters for XGBoost model, hyperparameters not listed are kept as default

subsample	1.0
reg_lambda	2.0
reg_alpha	0.1
n_estimators	300
max_depth	5
n_estimators	200
learning_rate	0.2
gamma	1
colsample_bytree	1.0

3.5 Speed loss model

The speed loss model is the centre of the calculation process, which predicts the involuntary speed loss caused by the weather and wave environment. A schematic overview of the calculation process of the developed code is presented in Fig. 3.9. The constraint of the developed speed loss model is the torque limit of the engine. It is derived from a combination of delivered power, P_D, at a certain rpm in the operating speed range according to Eq. 3.19. The torque limit creates a constant threshold applicable over the whole speed range in comparison to a limit on power, which is dependent on engine rpm.

$$Torque\ limit = \frac{P_D * 60}{n_{rpm} * 2\pi} \tag{3.19}$$

The input to the model is, apart from the ship characteristics, consists of the environmental parameters describing the sea state and wind, together with the speed cap. The speed cap is an operating speed limit that the ship is not allowed to exceed, even if there is margin to the torque limit. This is a way of moderating the fuel consumption.

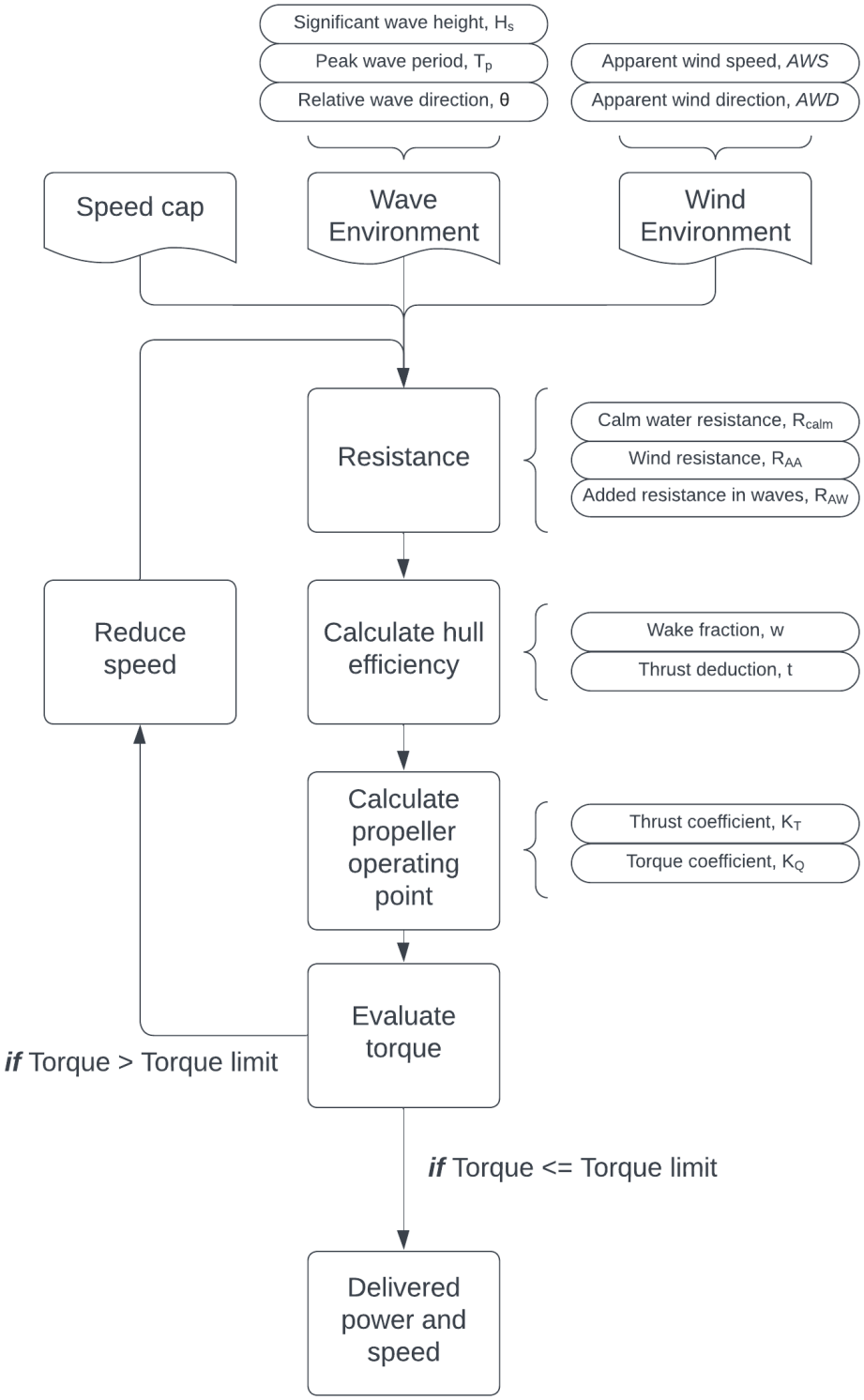

Figure 3.9: Schematic view of the speed loss model at one sampling point along the route

The procedure of evaluating the resistance is presented in Section 3.5.1.

When the script has run through all steps, it checks whether the torque limit is exceeded or not. If it is below the threshold, the delivered power and speed are calculated; if not, the speed is reduced, here in steps of 0.2 knots, and the calculations start again. The step of 0.2 knots is a relatively coarse resolution; however, it is necessary to maintain feasible computational times.

The speed loss model is a script that performs calculations and predicts the power and speed at one point along the route. The model is then utilised in a bigger perspective in the performance evaluation, described in Section 3.5.2.

3.5.1 Resistance and propeller calculations

The calm water resistance can theoretically be calculated in any preferred method. The accurate sea-trail data, previously discussed in Section 3.3.3 for assessing calm water resistance, is only valid for that ship design. Since the focus of this thesis is to investigate the performance of possible new ship designs, this is no longer valid. Therefore, the calm water resistance is calculated through the widely used empirical formula from Holtrop and Mennen (1982) previously explained in Section 3.3.3.

The wind resistance follows the same methodology as described in Section 3.3.3 in accordance to ITTC (2024).

Apparent wind speed and apparent wind direction are due to their nature being vector addition, a function of the ship's speed. A higher ship speed will twist the apparent direction closer to headwind than the true wind direction. Here, the apparent wind speed and apparent wind direction are calculated outside of the speed loss loop under the assumption that the speed is fixed at the speed cap. This is reasonably valid as long as the achieved speed is not too far from the speed cap. Since the change is AWS and AWD is relatively small, and that R_{AA} is small in comparison to R_{AW}, it is assumed to introduce an insignificant error to the overall predictions.

The added resistance in waves can also be calculated with any preferred model.

The results in this thesis are generated using the standard SNNM. The reason for not using the improved model is further discussed in Section 4.2.4 and Section 5.1.2, together with results from Section 4.2, which indicate that the machine learning model captures trends that are not intended. The correction term is found to be in the same order of magnitude as the R_{AW} as calculated by the SNNM, the uncertainty is large, and the model is suspected to be unreliable for extrapolation to new designs.

The code has two options on how to calculate the hull efficiency, η_H, through the wake fraction and thrust deduction factor. This can be provided through either the formulae from Holtrop and Mennen (1982) or custom formulae that uses data from Stena's model test of the IMOIIMAX hull. The results generated in this thesis utilise the custom IMOIIMAX formula.

The propeller curves are obtained from the Wageningen B-Series propellers and with dimensions and ratios according to Stena's preference. The torque limit is specified by Stena.

3.5.2 Performance evaluation

The speed loss model previously explained is used to evaluate the performance of a ship along a route with corresponding weather from the hindcast weather data. Performance is here quantified by the total energy demand along the route and the average achievable speed. The script takes two or more ports as input and generates a route in-between.

The route is created using the external SeaRoute function, which generates a set of samples containing waypoints along the route. For each waypoint, the weather data needed for the speed loss model is extracted and then passed on to the speed loss model. For every sampling point, the main output is the delivered power and achievable speed. By calculating the distance to the next waypoint and combining it with the achievable speed, the energy and time to the next waypoint can be estimated.

The total energy for the route is then calculated as the sum of all energies between the waypoints. The same goes for total time and distance. The average achievable speed is calculated from the total time and distance.

3.5.3 Assumptions

- The AWS and AWD is for each waypoint, constant within the speedloss model. It is calculated once in every waypoint with the ship velocity equal to the speed cap. This means that when the speed is reduced, the AWS and AWD remain the same as in the first iteration.

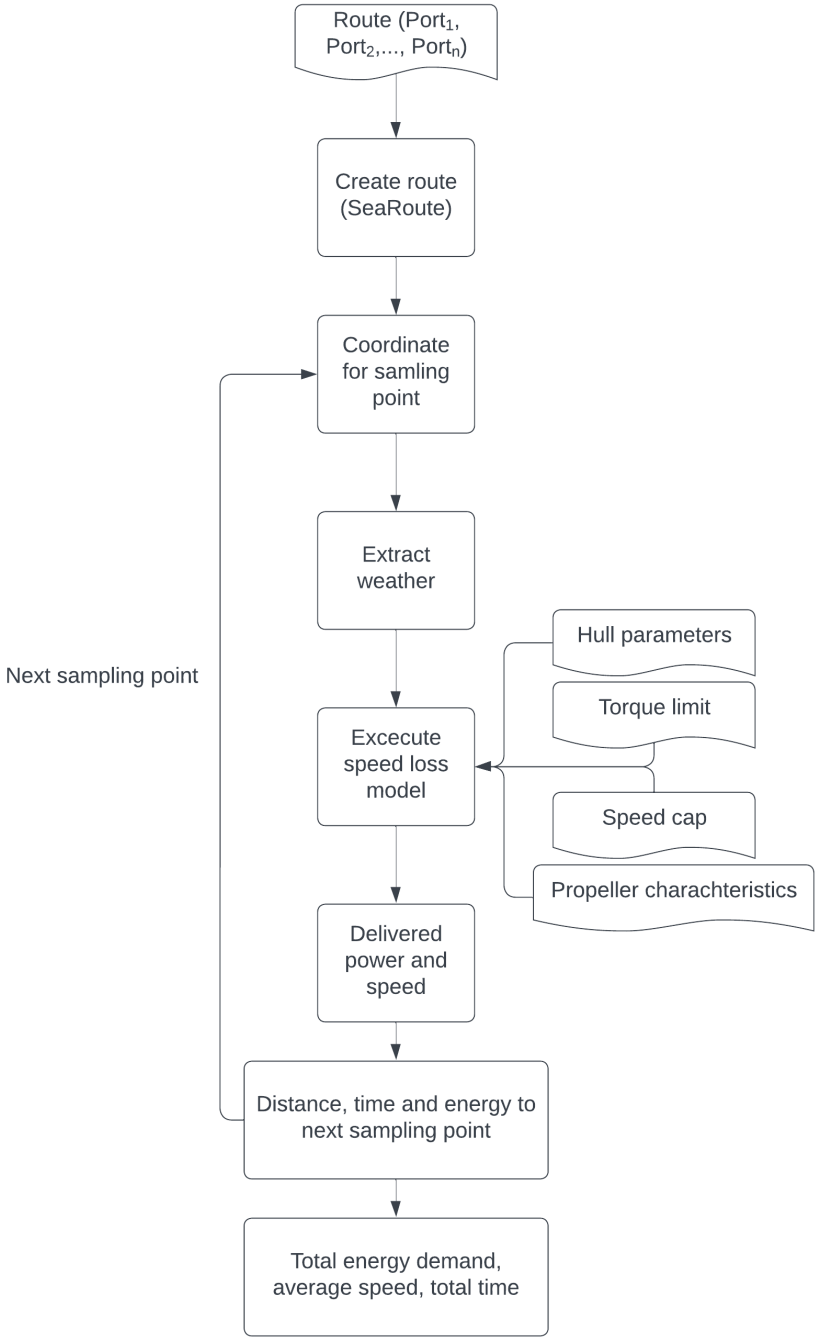

Figure 3.10: Schematic overview of the performance evaluation model between specified ports.

3.6 Optimisation

The optimisation is performed to find the optimum design, yielding the lowest energy consumption. Stena wants to find the optimum combination of Lpp, B, and T for a given displacement. The design and contract speed is set as 12 knots, and the displacement is slightly higher than the IMOIIMAX reference vessels. All studied designs, except for the already existing reference vessel, will have the same displacement.

The range of the main dimensions studied by this thesis are:

- $170 \leq L_{pp} \leq 190$ m
- $31 \leq B \leq 34$ m
- $10 \leq T \leq 13$ m

The intervals must be within a feasible limit such that the dimensions are not too extreme or different from today's IMOIIMAX design, both from an operational point of view and ensuring the validity of correction models and assumptions to hold.

The performance of the ship along a route, with real weather data in every waypoint, is not a simple function, where the parameters can be optimised through simple optimisation procedures.

The optimisation is, therefore, in this thesis, Monte Carlo-based. This implies that a large number of samples is generated and evaluated. The overview of the optimisation procedure is displayed in Fig. 3.11

The sample generation procedure, displayed in yellow, is further explained in Section 3.6.1. The pink box, where hull parameters are generated, is further explained in Section 3.6.2. The design evaluation, blue in the figure, is described in Section 3.6.5, which utilises the performance evaluation model previously described in Section 3.5.2 . Post processing of the results, the green box, is further explained in Section 3.6.6

It is important that the optimisation is on representative terms, since there is a big difference in ship design depending on routes, operational speed and encountered weather. The comparison of designs also needs to be on fair terms.

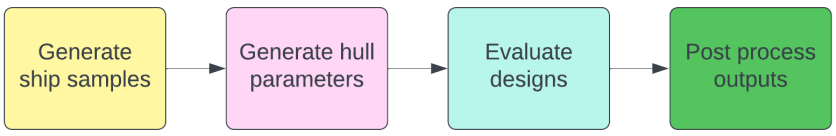

Figure 3.11: Overview of the four steps in the optimisation process.

3.6.1 Generating sample

The design samples must be generated for the Monte Carlo simulations. Since all designs should have the same displacement, ∇, the block coefficient is considered a free variable.

As a criterion, the Block coefficient must be below 0.85.

The sample size must be large enough to cover most of the design domain but yet small enough to be computationally possible on desktop computers.

Fig. 3.12 shows the randomly generated samples for different sample sizes. The lack of samples in the lower left corner is an effect of the upper limit on C_B. For this thesis, results are generated using a sample size of 200.

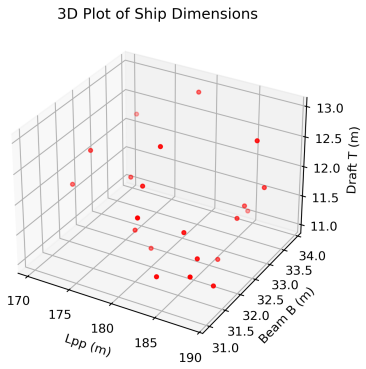

(a) Size 20

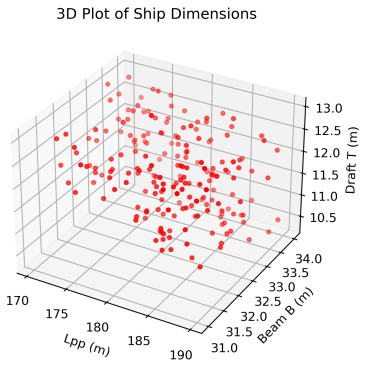

(b) Size 200

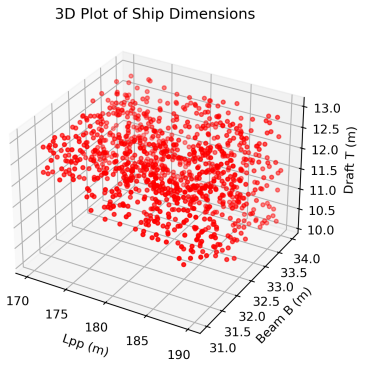

(c) Size 1000

Figure 3.12: Three different sample sizes with L_{pp}, B and T plotted in the three dimensional domain.

3.6.2 Generate hull parameters

The models included in this methodology need more information about the hull form than what is provided by the three main dimensions in the random samples. The parameters needed are presented in Table 3.6

Table 3.6: Parameter usage in SNNM and Holtrop and Mennen (HnM).

Parameter	SNNM	HnM
L_{pp}	×	×
L_{WL}		×
C_B	×	×
B	×	×
T_a	×	×
T_f	×	×
K_{yy}	×	
E_1	×	
E_2	×	
LCB		×
C_m		×
C_P		×
WPA		×
WSA		×
ABT		×
hB		×
A_T		×
C_{stern}		×
C_{bulb}		×
S_{APP}		×
App type index		×

- **Lpp**
  This parameter is a design variable, part of the generated sample.

- **LWL**
  LWL will be taken proportional to Lpp with the same relationship as the initial design.

- $\boldsymbol{C_B}$
  C_B is for a given combination of ∇, L_{pp}, B and T given by the definition:

$$C_B = \frac{\nabla}{L_{pp}BT} \tag{3.20}$$

  In order to improve the accuracy of the generated parameters, further assessed in Table 3.6.2, another empirical C_B is calculated and used as a temporary variable for approximation of the remaining parameters.

$C_{B,emprical}$ is given by Schneekluuth and Bertram as stated by (Parsons 2003)

$$C_{B,emprical} = 0.70 + 0.125 \tan^{-1}\left(\frac{23 - 100Fn}{4}\right) \tag{3.21}$$

- **B**
  This parameter is a design variable, part of the generated sample.

- $\boldsymbol{T_a, T_f}$
  This thesis only assesses even keel and thus no trim. The draft at the fore and aft perpendicular will therefore be equal to T which is a design variable.

- $\boldsymbol{k_{yy}}$
  The pitch radius of gyration, k_{yy}, is a measure of how the mass is distributed around the pitch axis. This measure is relatively constant among a broad range of vessels and will, for this thesis, have a constant value of $k_{yy} = 0.25L_{pp}$

- $\boldsymbol{E_1}$
  The entrance angle E_1 is calculated from the length of the entrance, which is the length of the waterline where the waterplane width reaches $0.99B$. In this thesis, the length of the entrance is kept proportionally constant with regards to L_{pp}, with proportions as the IMOIIMAX design.

$$E_1 = arctan\frac{0.495B}{L_E} \tag{3.22}$$

- $\boldsymbol{E_2}$
  The angle of the run E_2 is calculated from the length of the run, which is the length of the waterline, measured from the aft where the waterplane width reaches $0.99B$. In this thesis, the length of run is kept proportionally constant with regards to L_{pp}, with proportions as the IMOIIMAX design.

$$E_2 = arctan\frac{0.495B}{L_R} \tag{3.23}$$

- ***LCB***
  The longitudinal centre of buoyancy, LCB, is a measure of where, in the longitudinal direction, the centre of immersed volume is. Often measured from midships. Faster ships tend to have LCB further aft than slower ships.

  This is approximated through Harvalds formula presented in Parsons (2003).

$$LCB = 9.7 - 45Fn \pm 0.8 \tag{3.24}$$

- $\boldsymbol{C_M}$
  The midship section coefficient, C_M is calculated from Schneekluth and Bertram as presented in Parsons (2003)

$$C_M = 1.006 - 0.0056C_{B,emprical}^{-3.56} \tag{3.25}$$

- ***C_P***
  The prismatic coefficient is derived from the definition.

$$C_P = \frac{C_B}{C_M} \tag{3.26}$$

- ***WPA***
  The waterplane area, WPA, is calculated from the definition where C_{WP} is obtained using the Schneekluuth and Bertrams formula for tankers and bulk carriers presented in Parsons (2003).

$$WPA = C_{WP} * L_{WL} * B \tag{3.27}$$

$$C_{WP} = \frac{C_{B,emprical}}{0.471 + 0.551 C_{B,emprical}} \tag{3.28}$$

- ***WSA***
  The Wetted Surface Area, WSA is evaluated using the formula from Holtrop and Mennen (1982), where ABT is the transverse sectional area of the bulb at the position where the still-water surface intersects the stem.

$$WSA = LWL(2T + B)\sqrt{C_M}(0.453 + 0.4425\, C_{B,emprical} \tag{3.29}$$

$$- 0.2862\, C_M - 0.003467\, B/T + 0.3696\, C_{WP}) \tag{3.30}$$

$$+ 2.38\, \frac{A_{BT}}{C_{B,emprical}}. \tag{3.31}$$

- ***ABT***
  The transverse sectional area of the bulb, ABT, is kept constant with the same value as the IMOIIMAX design.

- ***h_B***
  The position of the centre of ABT above the keel line, h_B, is kept constant with the same value as the IMOIIMAX design.

- ***A_T***
  The immersed transom area, A_T will be kept constant with the same value as the IMOIIMAX design.

- ***C_{stern}***
  Holtrop and Mennen (1982) introduces a stern coefficient, C_{stern} depending on the aftbody form. Values are given by Holtrop and Mennen (1982) and presented in Table 3.7. In this project, Stena's custom value, based on experience, is used.

- ***S_{APP}***
  The wetted area of appendages, $\boldsymbol{S_{app}}$, is assumed to be constant as of the IMOIIMAX vessels.

- **App type index**
  The appendage type index follows the classification as of Holtrop and Mennen (1982). Here index one is rudder behind skeg, index two is rudder behind stern, etc.
  For this thesis, index two is used.

Table 3.7: Values for the stern coefficient as presented by Holtrop and Mennen (1982)

Aftbody form	C_{stern}
V-Shaped sections	-10
Normal section shape	0
U-shaped sections (Hogner stern)	10

Accuracy of generated parameters

In order to evaluate if the generated parameters following the above procedure give reliable results, they are tested on the input variables from the IMOIIMAX and see if the other variables are close to what the design is. In Table 3.8, the relative values of $X_{calculated}/X_{actual}$ are presented.

Table 3.8: Accuracy of generated parameters using the standard empirical formulas

Parameter	**Relative value**
$C_{B,empirical}$	$+5\%$
C_M	-0.3%
LCB	$+0.8\%$
WPA	-1.4%
WSA	-0.2%

It can be seen that the $C_{B,empirical}$ does not match well. Therefore, a second "parallel" method is employed where the displacement is fixed, giving a correct C_B through definition, but using the empirically calculated C_B for the calculations of the other parameters since they had a good match.

3.6.3 Fair comparison of designs

To give a fair comparison of different hull designs, each hull will be deployed at the same routes, with the same weather. A slower vessel will consume less energy, and thus, to compare them on equal terms, they are forced to have the same sailing time, i.e., the same average achievable speed. This is achieved by tuning the speed cap, the virtual speed limit explained in Section 3.5. A ship that has a higher involuntary speed loss will have to compensate and operate at higher on other parts of the route. This will prevent bad (slow) designs from being promoted.

The simulations will, for this thesis, run on "frozen" weather. The weather is selected from one time instance in the weather data, and then does not change with time as the ship advances along the route.

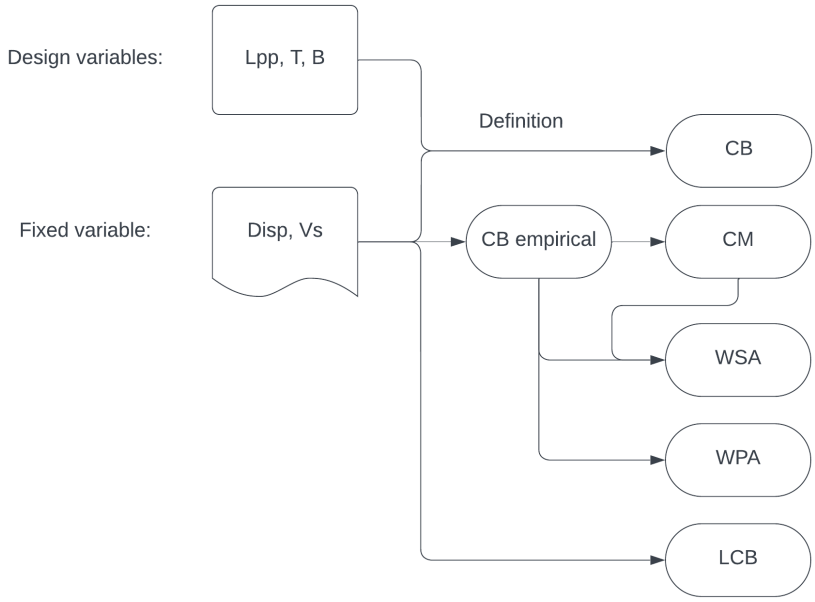

Figure 3.13: Adapted methodology of calculating parameters of a new ship design

This ensures that the wave and wind data will be the same for all voyages in all positions, which makes comparison valid. If the timestamp were to be simulated, there is a risk of running into an unfair optimisation. There is a possibility of a slower ship being "lucky" by avoiding rough weather conditions because the time stamp is different.

The optimisation will not include ocean currents, and the ship's STW will therefore be assumed to be equal to SOG. The reason for this is that currents affect all ships equally, and it is therefore not a relevant factor to include in an optimisation procedure.

The hull parameters for the reference hull will be generated using the same procedure as the other samples, even though the data is available at Stena. The reason for this is that the comparison should be fair.

3.6.4 Routes and weather

The routes should represent what the ship is expected to trade on during its lifetime, as the routes will influence the encountered weather. A ship, for example, sailing between Europe and North America will most likely encounter more severe sea states than a ship sailing in the Indian Ocean. Fig. 3.14 shows a selection of the ports that Stena Immortal traded to during the period 2020-2024. It can be seen that it has a global trading pattern. The routes used in this thesis are presented in Table 3.9. The weights used for the different routes are not disclosed.

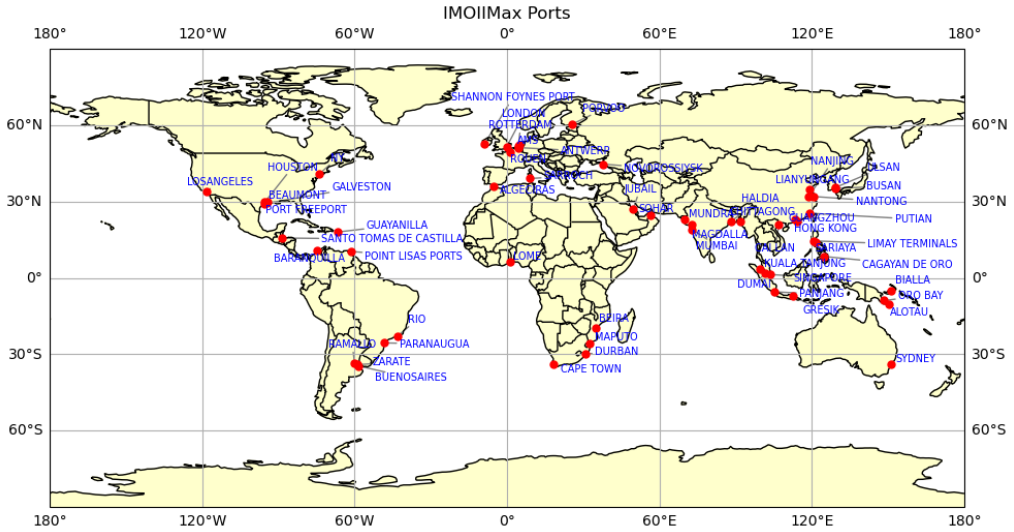

Figure 3.14: A selection of ports that STENA IMMORTAL traded to in the period 2020-2024 (S&P Maritime 2025).

Table 3.9: Selected routes with departure and arrival ports.

Route #	Departure	Arrival	Route length [NM]
1	Amsterdam	New York	3246
2	Amsterdam	Lome	4104
3	Sarroch	New York	3826
4	Houston	Amsterdam	4956
5	Houston	Pozos Colorados	1896
6	Houston	Los Angeles	4476
7	San Lorenzo	Mundra	8316
8	San Lorenzo	Chittagong	9051
9	Jubail	Rotterdam	6494
10	Jubail	Durban	4010
11	Singapore	Sydney	4068
12	Busan	Singapore	2544
13	Singapore	Amsterdam	8360
Total length			64347

Since the methodology is based on hindcast weather data and not global wave statistics, the simulations need to include as many different time instances of weather as possible. However, this is not feasible when comparing a large number of ship samples. Therefore, two weather instances will be selected, one representing winter and one summer (northern hemisphere).

The times for weather will not be selected completely at random since the model does not feature weather routing and cannot avoid storms. Therefore, dates are chosen that feature weather that can be expected at this time of year.

2024-07-10-1200

To represent summer, a day in July is selected. The weather and routes sailed are presented in Fig. 3.15. This time instance features calm weather on the Atlantic Ocean but some rough patches with wave heights up to 8 meters outside of Durban. This area is just about avoided due to the routing tool, SeaRoute, keeping close to the coast. However, waves up to $\sim$5 m are encountered further west along these routes.

2025-01-02-1200

A day in January is selected as representative for winter weather and presented in Fig. 3.16. This time instance features wave heights up to six meters along three of the routes across the Atlantic Ocean. One of which traverses in a west-east direction and thus features head waves. The southern hemisphere has calm weather, and most of the routes have wave heights not exceeding 3 meters.

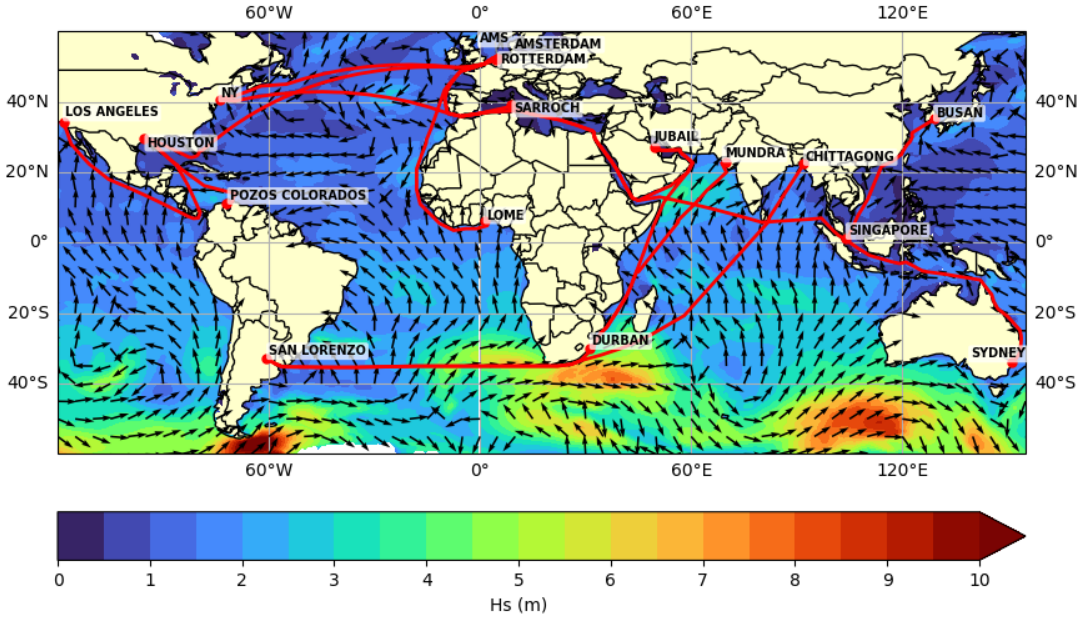

Figure 3.15: Evaluated routes together with wave height and wave direction at 2024-07-10-1200.

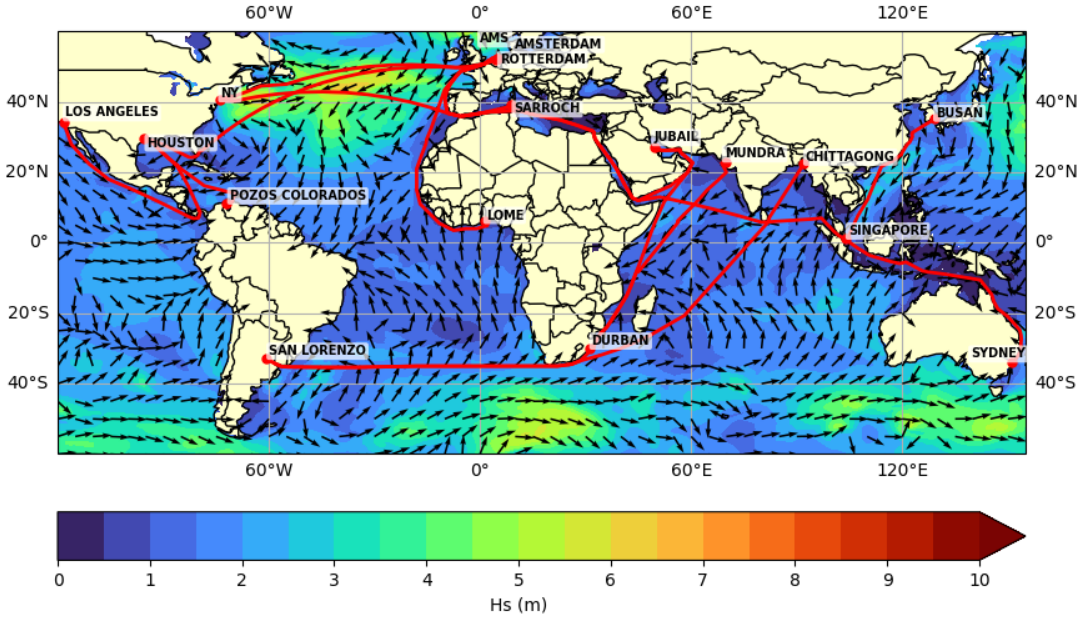

Figure 3.16: Evaluated routes together with wave height and wave direction at 2025-01-02-2000.

3.6.5 Evaluate designs

The core procedure of this optimisation is to evaluate all designs from the generated samples. Per previous sections, it is important with a fair evaluation and comparison. All ships should maintain the same average speed of 12 knots. A schematic overview of the evaluation procedure is presented in Fig. 3.17

Here, all ships are tested on all routes. The model runs a ship, with an initial speed cap on the entire route, then evaluates the average speed. If the average speed is too low, it increases the speed cap, and if it is too high, it reduces the speed cap. When a satisfactory average speed is achieved, the performance data is written to the output file for all ships on that route. If the ship, regardless of speed cap, cannot achieve the average speed specified. It is noted as a fail. The failed samples can then be processed separately later, as these will fail to maintain the average speed, usually set by the chartering contract.

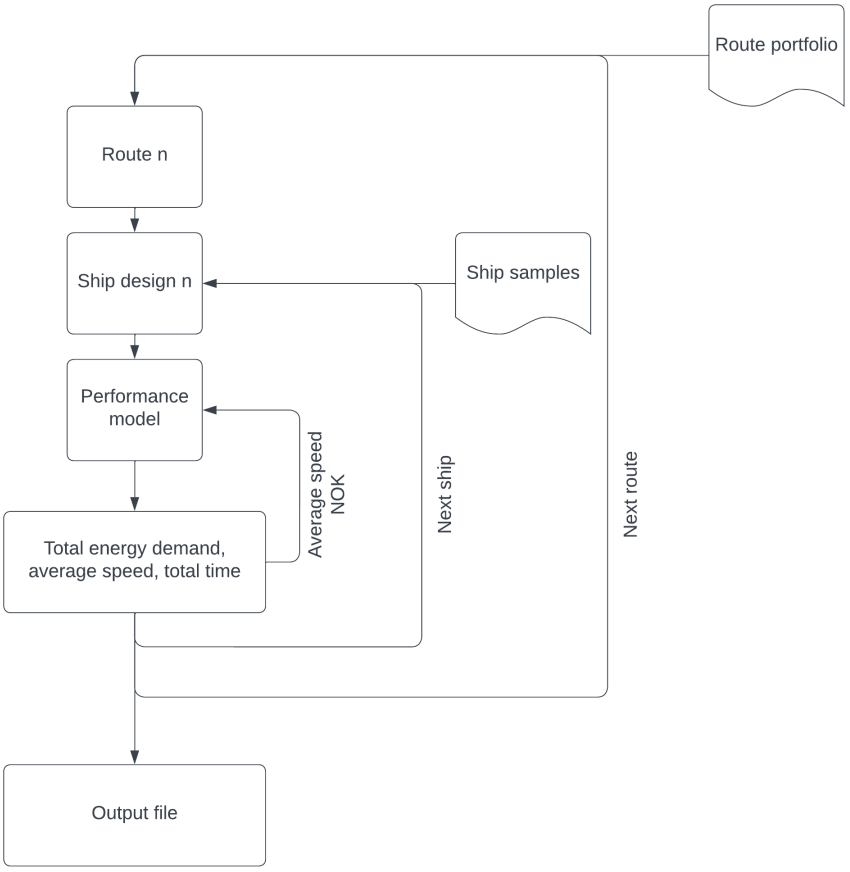

Figure 3.17: Schematic overview of the evaluation procedure. (NOK=Not okay)

The performance values that are extracted in the evaluation are:

- Total energy [kWh]
- Total time [h]

- P_D at design speed [KW]
- Average R_{AW} [N]
- Average instantaneous R_{AW}/R_{calm} [-]
- Average speed [kn]
- Required speed cap [kn]

3.6.6 Post processing outputs

The output consists of 26 output files, one for each route and weather combination. Every file consists of data for all 200 samples.

The routes are weighted separately for the different weather conditions and then summed up, explained by Fig. 3.18. Using this method, the difference in optimum hulls for the separate weathers can be evaluated, and then the overall winner can be found by summing up the two results. The same procedure can be used, but for a larger amount of weather (time instances).

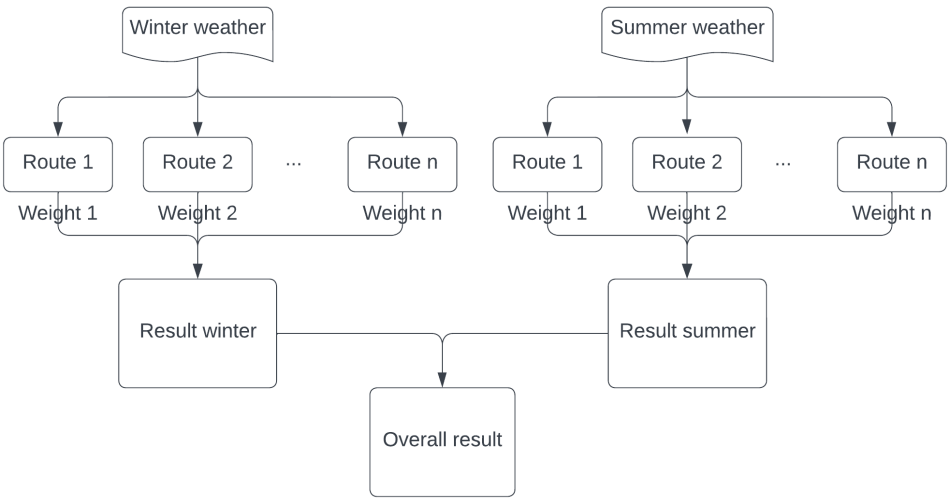

Figure 3.18: Procedure of post-processing output files.

3.6.7 Assumptions

The hull optimisation will only consider the laden condition on even keel. Ballast condition and/or a trimmed scenario will not be considered.

- Performance of laden condition and constant draft will be assumed to be representative for each hull design.
- Ocean currents are neglected, such that STW=SOG

- The lightweight is assumed to be equal for all designs, such that a constant displacement results in the same deadweight for all designs.
- The modified Holtrop and Mennen is assumed to be accurate for this vessel type; the details of this modification remain undisclosed.
- Course and bearing are assumed to be equal. This implies no leeway is present along the route.

4

Results

This chapter presents the results obtained using the methodologies described in Chapter 3. The results include an analysis of the voyage data together with a comparison of the accuracy obtained through the SNNM method with different models to approximate the correction. Here is also a detailed presentation of the optimum designs and indicated trends.

4.1 Voyage data analysis

The data supplied are from Stena Immortal, one of the 13 IMOIIMAX vessels operated by Stena Bulk, for the period 2024-06-24 to 2025-02-25. The data used in this project are explained more in Section 3.3, but include essential parameters for power prediction, speed, and some measured wind parameters. This section describes the data in more detail, while the applied method is described in Section 3.3.

4.1.1 Statistical distribution of operating conditions

To describe the operations and environment encountered for the voyages included in the data, some statistics are provided.

The distribution of the speed over ground for the dataset is presented in Fig. 4.1, which indicates that the ship is operating mainly at speeds around 12.5 kn, note that these statistics are after filtering the data to only include transport and not leaving or entering ports. Values less than 11 knots are not included.

Fig. 4.2 shows the distribution of the significant wave height during the time period covered by the voyage data. Here, a peak is seen at approximately 1.5 meters, and waves exceeding 3 meters are rarely seen.

The peak wave period, T_p is distributed according to Fig. 4.3.

Wave peak period, T_p and significant wave height, H_s are combined, by common practice, into a wave scatter diagram. The wave scatter diagram for the analysed voyage data is presented in Fig. 4.5.

The direction in which the ship encounters the waves is illustrated in Fig. 4.4, where 0°is the bow and 180°is the aft, in the clockwise direction.

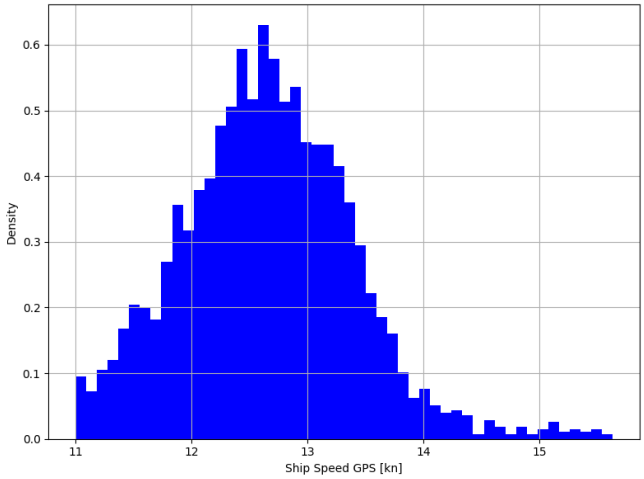

Figure 4.1: Distribution of speed over ground

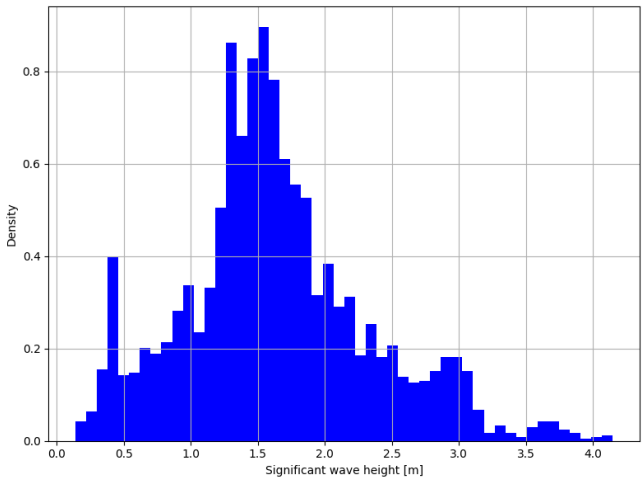

Figure 4.2: Distribution of significant wave height.

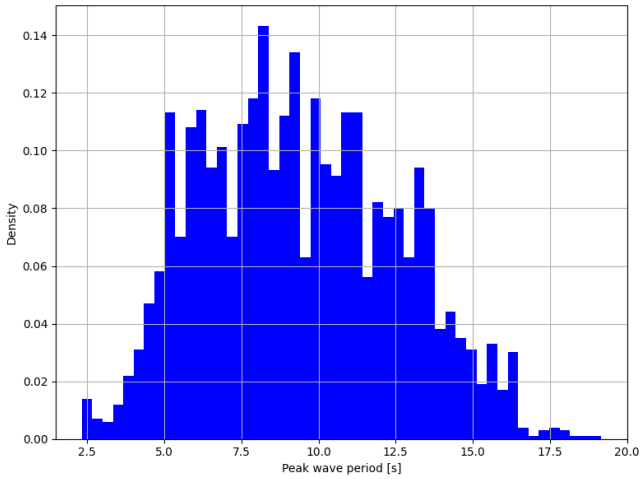

Figure 4.3: Distribution of peak wave period.

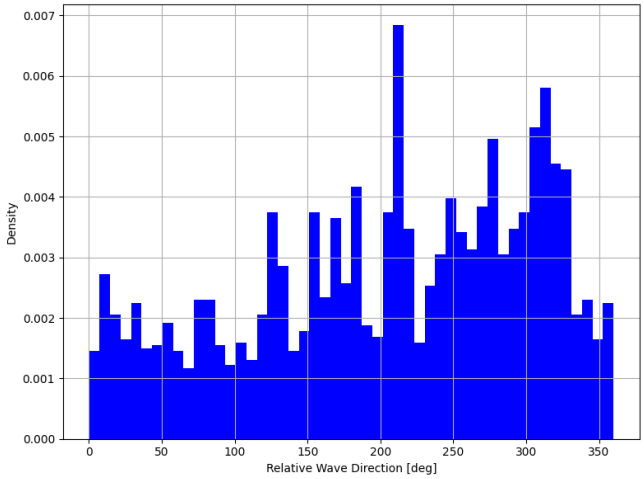

Figure 4.4: Distribution of relative wave direction.

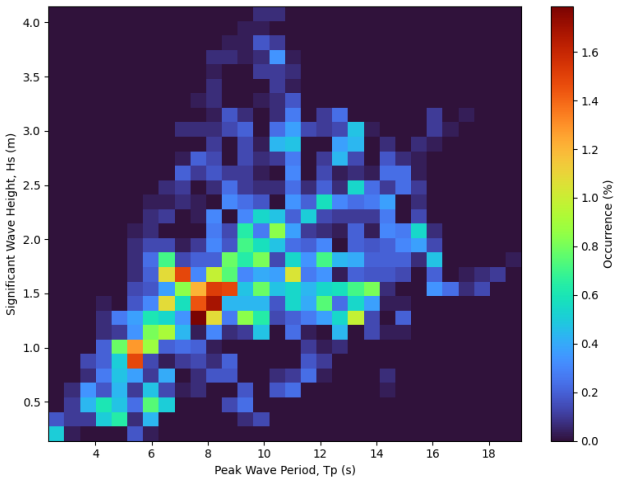

Figure 4.5: Wave scatter along the measured voyage.

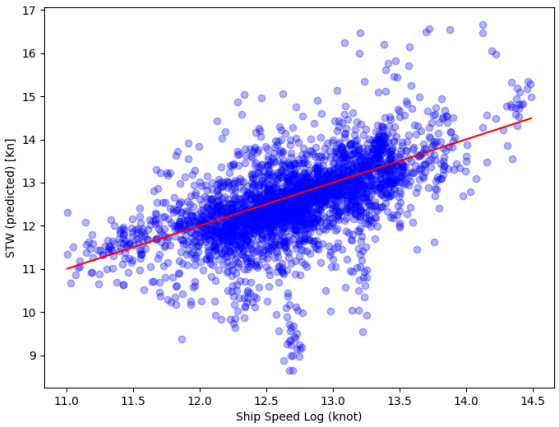

Figure 4.6: Correlation of calculated and measured STW.

These figures show that the ship encounters many different conditions, and especially Fig. 4.4 illustrates that the wave direction is distributed around the ship and must be considered from every angle.

4.1.2 Ocean currents and speed through water

Measured Speed Through Water (STW) is available, but there are large uncertainties regarding measurement errors or calibration. The STW is measured at the hull surface, i.e., the boundary layer is measured and not the far field velocity. The STW is also calculated as described in Section 3.3 and compared to the measured data. The calculated STW (predicted) compared to the ship's measured log speed is compared in Fig. 4.6.

The pointwise error has a median of -0.12 and standard deviation of 0.77, i.e., the calculated speed through water is often lower than what is measured, but overall, the prediction is decent. It was decided to use the measured STW for the calculations done using the voyage data.

4.2 Accuracy of SNNM and improvement of the model

The machine learning is supposed to model the difference between the modelled and the "measured" R_{AW}. In Fig. 4.13 added resistance calculated using the SNNM method is plotted against the added wave resistance based on the voyage data.

4.2.1 Accuracy of initial model

An important aspect of the accuracy is how each parameter influences the resistance. An investigation is made to see the correlation between environmental and ship variables and the resulting added resistance in waves, both measured and calculated using the SNNM method.

The ship speed has a large effect on the added resistance in waves, Fig. 4.7 shows that the trend is similar, but the SNNM method gives generally smaller values for the added resistance in waves. The measured added resistance also goes below zero at times, whereas this never happens when the SNNM method is used. The added resistance in waves is low when the speed is high; this is because when the ship travels at high speed, it is because the wave environment allows it, hence the added resistance is low at high speeds.

The significant wave height is an important wave parameter that affects the resistance. The SNNM method relies heavily on the significant wave height, as can be seen in Fig. 4.8. However, the measured added resistance in waves has a more uncorrelated distribution. This could indicate that the added resistance in waves is not extracted correctly from the measurements or that there are other factors that have a large effect on the resistance, which are not captured.

Other wave parameters that affect the resistance are the wave period, in this case, the peak wave period. Fig. 4.9 illustrates this. The higher values for added resistance in waves, both for measured and using SNNM, are around or slightly below the wave period, which equals a wave length similar to the length of the ship's waterline.

The amount of resistance added by the waves depends on the angle at which the ship encounters the waves, as seen in Fig. 4.10. The SNNM method has a heavier dependence on the direction, especially on how following waves are treated. Another note is that the added resistance in waves extracted from the measurement parameters gives negative values for waves encountered in more than only the following direction.

Wind resistance, or air drag, is calculated and deducted from the total resistance to retrieve the added resistance in waves from the measurement data. It is therefore important to look at how the wind affects the resistance. As seen in Fig. 4.11, an increase in wind speed has a small correlation with the added resistance; this is likely due to the correlation between wind force and wave height.

Fig. 4.12 indicates that the head wind correlates with increased added resistance in waves, again likely due to the correlation between the wind angle and wave angle.

Fig. 4.7 to Fig. 4.12 shows that the measured added resistance in waves and SNNM shares some trends. Overall, SNNM shows more correlation on the wave parameters, which might indicate that the measured added resistance captures some other resistances that are not intended.

An important aspect is to determine the accuracy of the SNNM model without modification. Fig. 4.13 show each point with calculated R_{AW} compared to what is measured, as described in Section 3.4. It can be seen that the measured added resistance in waves cannot be completely explained by the SNNM method, the R^2 - score is 0.148, which means that the model does not explain the data very well, which is unfortunate. This is due to uncertainties and other limitations in both the method and the measurements. The SNNM method was developed on a large database of ships in different conditions, and the data points in waves from beam and following seas were fewer, which could have led to a worse fit, especially if the ships containing these measurements were not medium-range tankers. In Fig. 4.13, it can be seen that the model often predicts a smaller added resistance than what is measured. This general trend could be explained by biofouling, which has a significant impact on ship resistance as explained in Section 2.1.4.

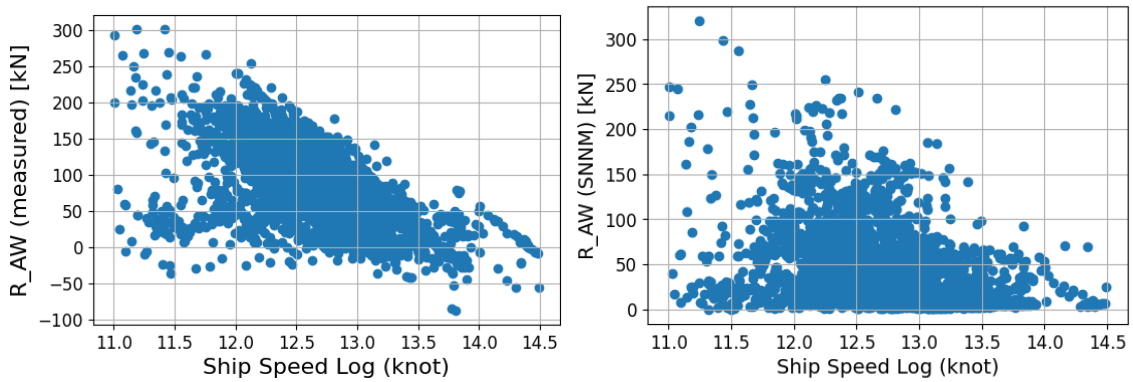

(a) Measured added resistance **(b)** Calculated added resistance

Figure 4.7: Added resistance as a function of ship speed

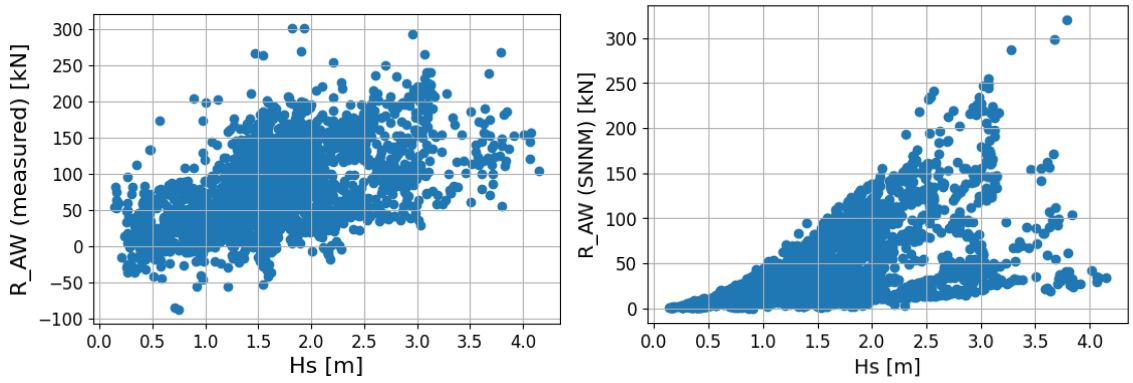

(a) Measured added resistance **(b)** Calculated added resistance

Figure 4.8: Added resistance as a function of peak wave period

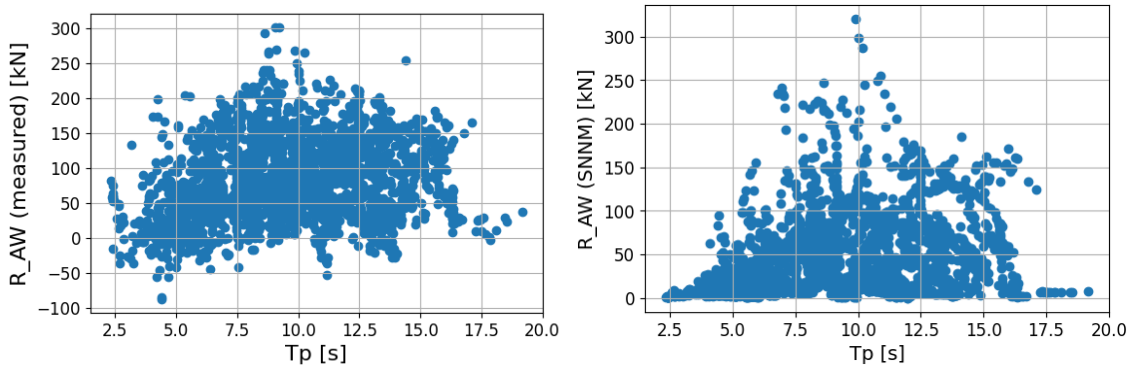

(a) Measured added resistance **(b)** Calculated added resistance

Figure 4.9: Added resistance as a function of peak wave period

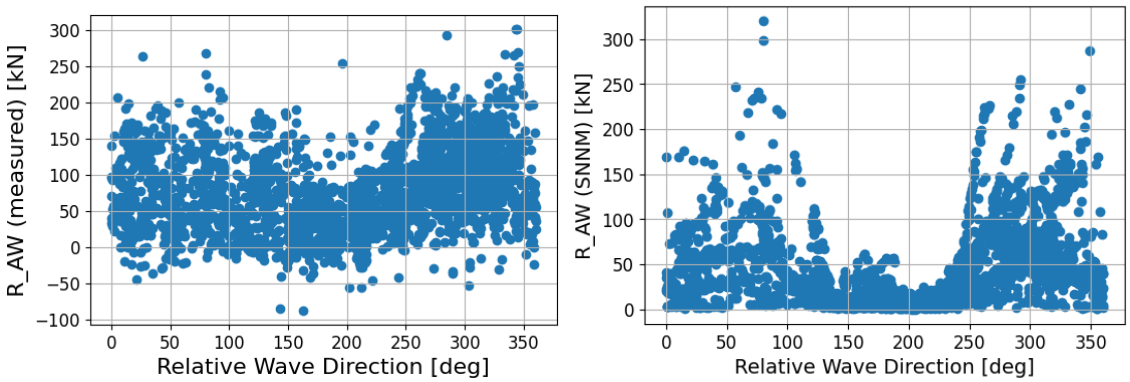

(a) Measured added resistance **(b)** Calculated added resistance

Figure 4.10: Added resistance as a function of relative wave direction

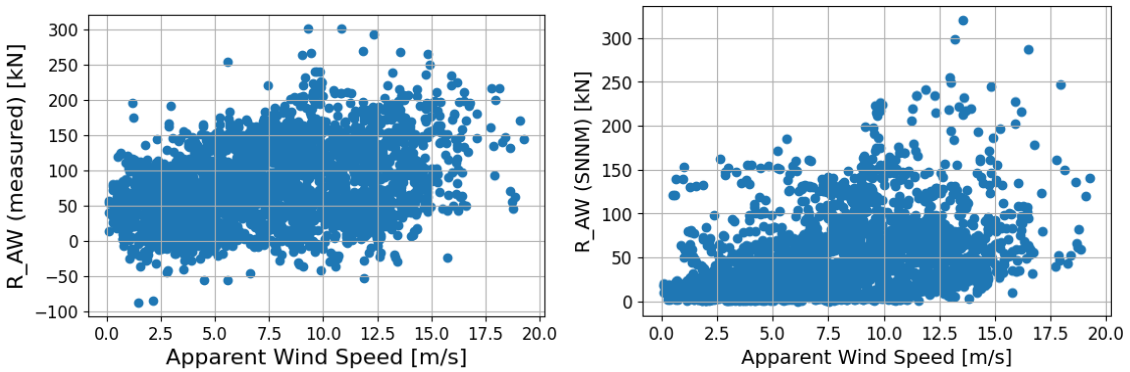

(a) Measured added resistance **(b)** Calculated added resistance

Figure 4.11: Added resistance as a function of apparent wind speed

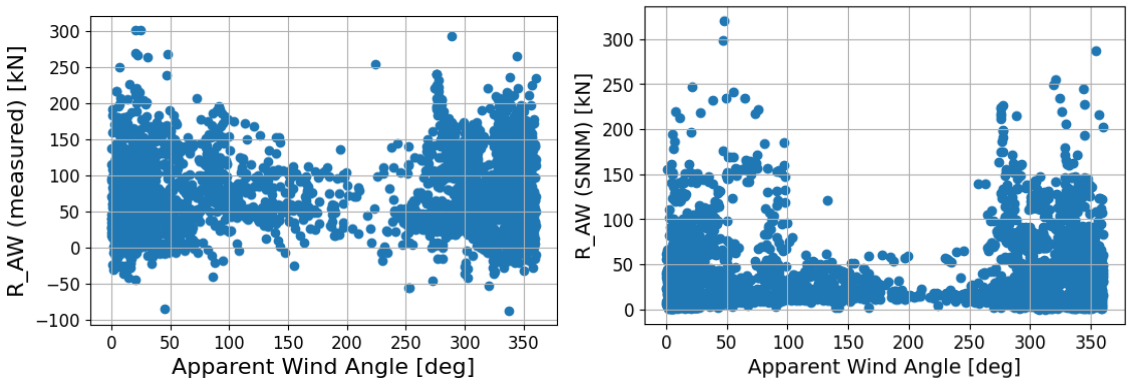

(a) Measured added resistance **(b)** Calculated added resistance

Figure 4.12: Added resistance as a function of apparent wind angle

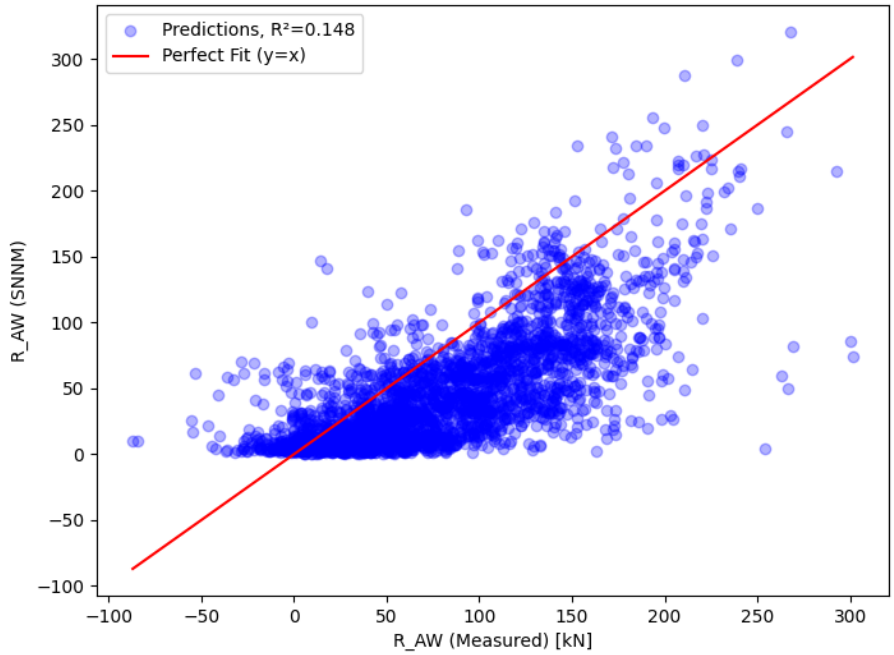

Figure 4.13: Comparison of calculated R_{AW} with approximated R_{AW} from measured data for the entire voyage.

The accuracy of the model is also highly dependent on the wave spectrum and what waves are included; the selected spectrum is modified Pierson-Moskowitz with spreading factor s = 75. In reality, this varies; it can also be argued that the wind waves and swell should be considered and calculated separately. However, to simplify calculations, the peak wave period is used and the significant wave height of combined wind and swell.

4.2.2 Whitebox model

The whitebox model is a linear regression model in which some input parameters are altered to better capture the nonlinearities of the problem. Table 4.1 shows the coefficients and intercept of the linear model. This is the main advantage of a linear model: it is transparent and less prone to unexpected predictions on new data.

This model gives an R^2-score of 0.295, the input parameters have been modified stepwise and, as presented in Table 4.1, gave the best result. The performance of the model on the test split of the data is illustrated in Fig. 4.14.

Adding the linear model for the error with the original SNNM gives improved results compared to the SNNM-model on its own. As seen in Fig. 4.15, compared to the SNNM model in Fig. 4.13.

The whitebox model is not very accurate on predicting the error, but combined with

Table 4.1: Coefficients and intercept for the linear whitebox model

Parameter	**Coefficient**
Mean Draft [m]	8.62
Hs [m]	-1.09
Tp [s]	0.337
STW^2 [kn^2]	-1.05
cos(Relative Wave Direction [rad])	-8.80
sin(Relative Wave Direction [rad])	-6.37
Intercept	**117.47**

the SNNM model, there is still a large improvement to be seen.

4.2.3 Accuracy of blackbox model

The two black box models studied are random forest regression and XGBoost. The random forest regressor gives good results in predicting the error, with an R^2 of 0.800, as seen in Fig. 4.16.

Combining the predicted error with the SNNM model gives an even better prediction of R_{AW} compared to the value calculated from the measurementsm, shown in Fig. 4.17.

The XGBoost is based on the random forest model, but implements some extra features, as explained in the theory. Fig. 4.18 shows the predicted error compared to the calculated error; the model gives an R^2 of 0.822, a slight improvement over the random forest model.

The small improvement in the predictions is also shown when combining the XGBoost model with SNNM, this gives an R^2 of 0.910 as seen in Fig. 4.19.

4.2.4 Use of improved models

The improved models are seen to have much better results than the standard SNNM. However, the correction, ε in:

$$R_{AW}^{corrected} = R_{AW}^{SNNM} + \varepsilon \tag{4.1}$$

is found to be in the same order of magnitude as R_{AW}^{SNNM}. This is unwanted and takes the model into unknown territory. Even if it is more consistent with the measured data, one can argue that instead of increasing the accuracy of the predicted R_{AW}, it compensates for measurement errors, assumptions, or other factors that are not considered in this thesis. One of these is biofouling.

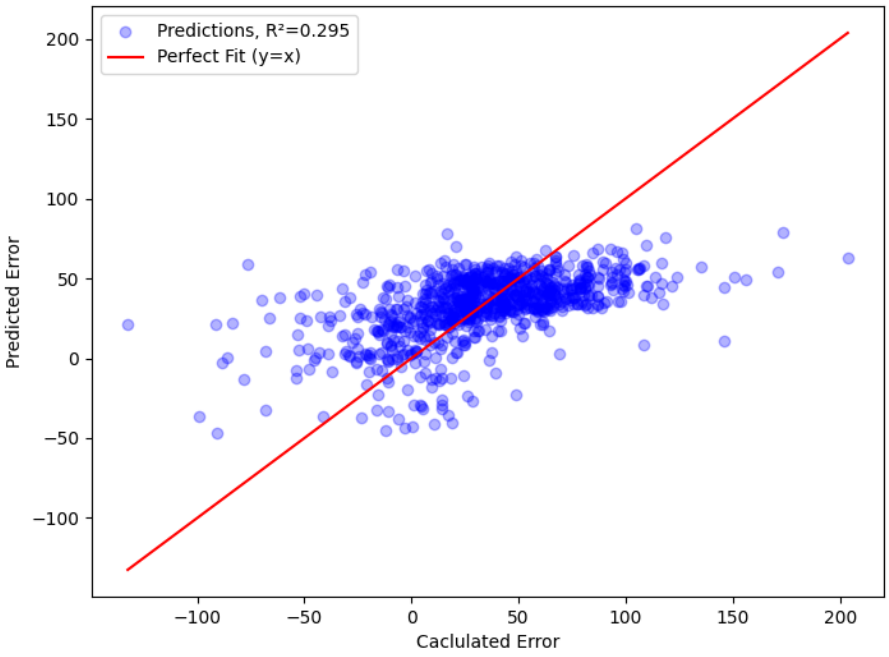

Figure 4.14: Comparison of error between calculated R_{AW} (SNNM) and measured, and the predicted error.

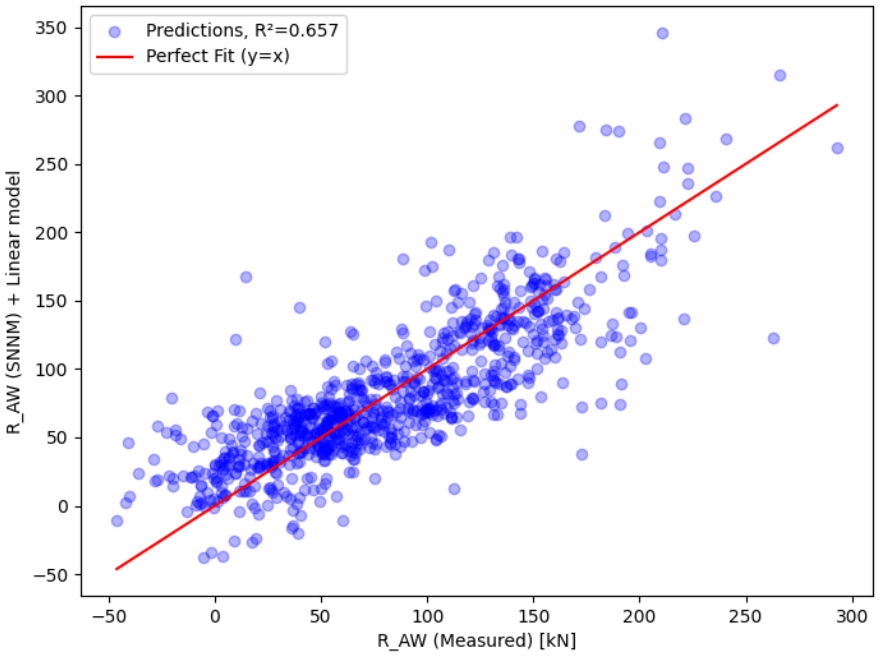

Figure 4.15: Comparison of calculated R_{AW} plus the regression model with approximated R_{AW} from measured data for the entire voyage.

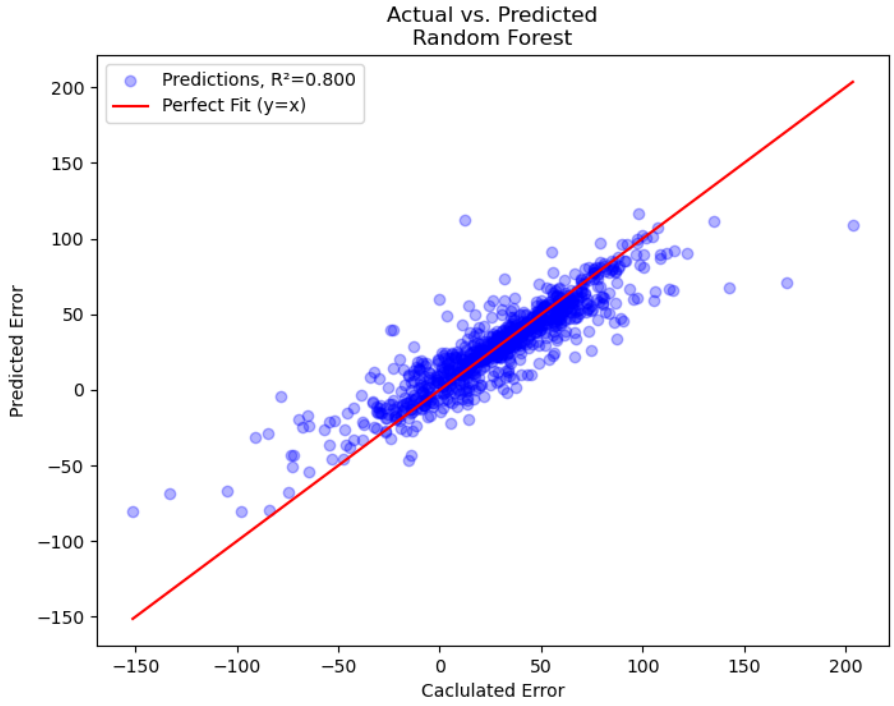

Figure 4.16: Comparison of error between calculated R_{AW} (SNNM) and measured, and the predicted error.

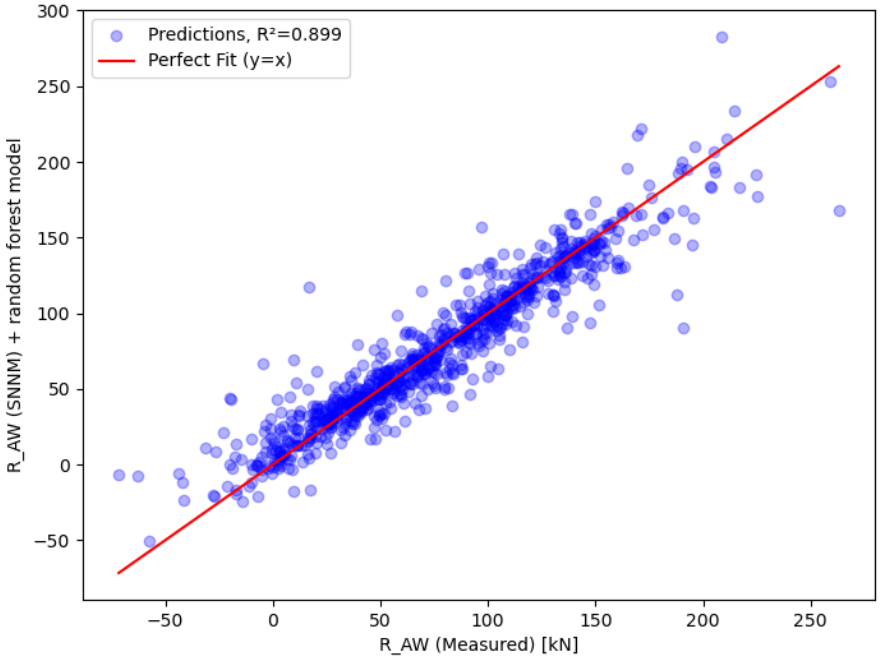

Figure 4.17: Comparison of calculated R_{AW} plus regression model with approximated R_{AW} from measured data for the entire voyage.

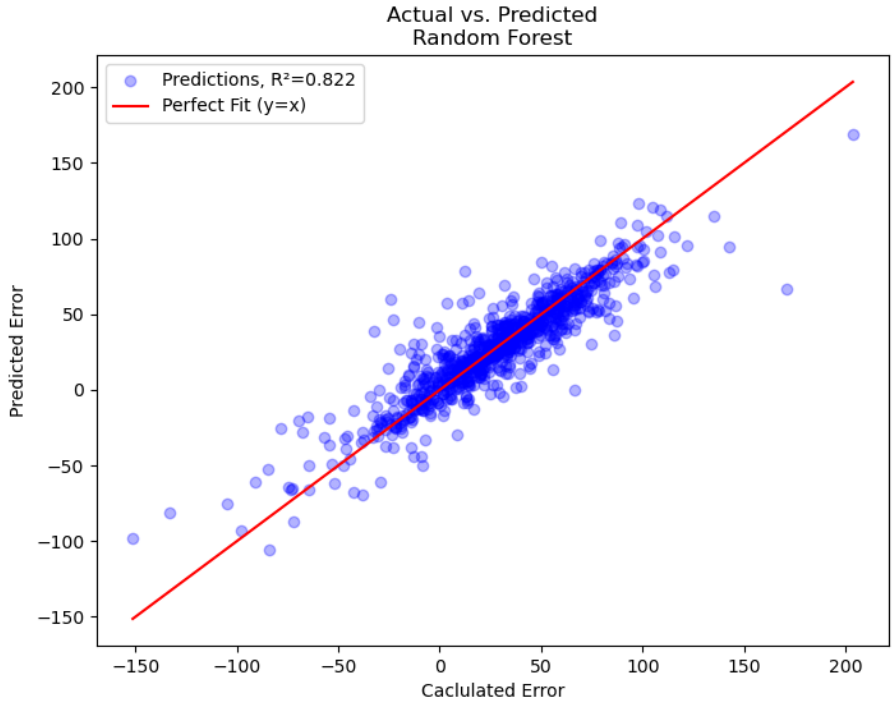

Figure 4.18: Comparison of error between calculated R_{AW} (SNNM) and measured, and the predicted error.

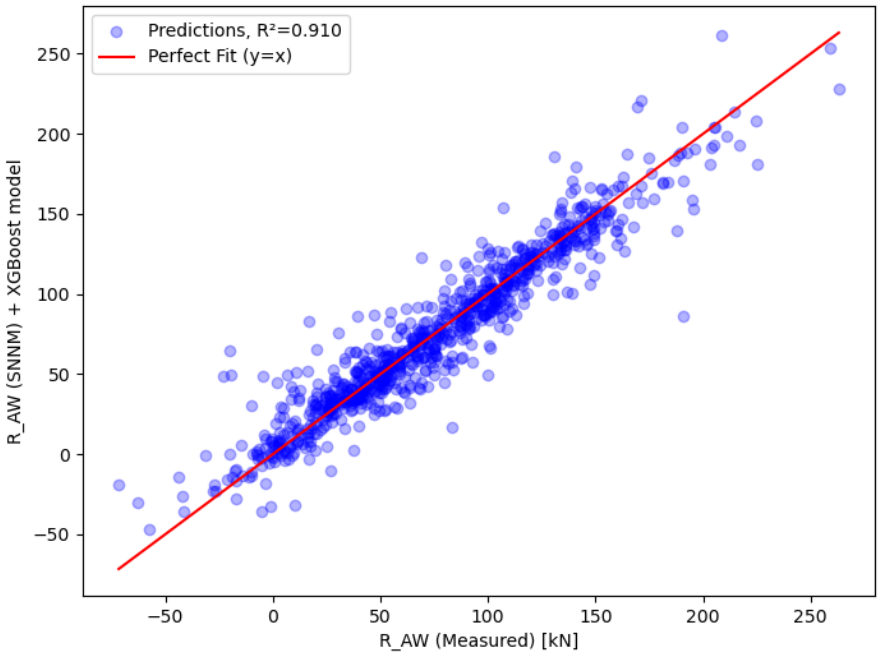

Figure 4.19: Comparison of calculated R_{AW} plus regression model with approximated R_{AW} from measured data for the entire voyage.

4.3 Route performance evaluation

The performance of all ship designs is evaluated and compared on 13 different routes for summer and winter. A more complete explanation of the procedure is previously included in Section 3.6. The routes studied and the weather encountered for the respective season is presented again in Fig. 4.20 and Fig. 4.21. To get a better understanding of the sailing conditions encountered, Table 4.2 presents the average speed cap and average required energy of all samples on each route and for summer and winter separately. It can be seen that most of the routes during summer require a speed cap of 12 or just above 12 knots to achieve an average speed of 12 knots. This is expected since the engine is dimensioned with a torque limit sufficient to reach contract speeds during the speed trial, which is several knots above the 12 knots that are the operating speed for this performance evaluation.

For all routes except Sarroch - New York and Houston - Amsterdam, all designs passed the speed requirement of 12 knots. For these routes, 171 and 201 of the designs, respectively, failed the criterion. Since this was an overall failure due to very bad sailing conditions, these designs are accepted and included in the results.

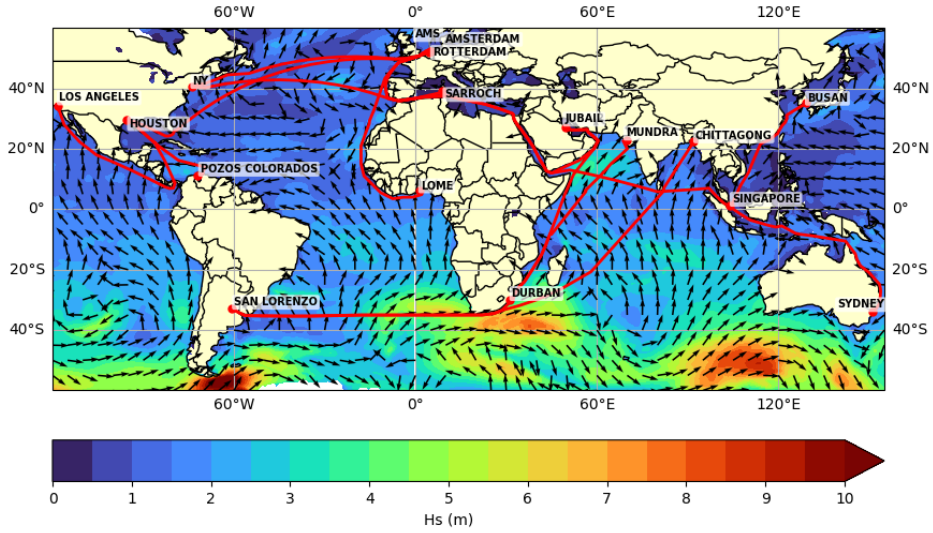

Figure 4.20: Routes for the optimisation plotted together with the weather representing summer (Northern hemisphere).

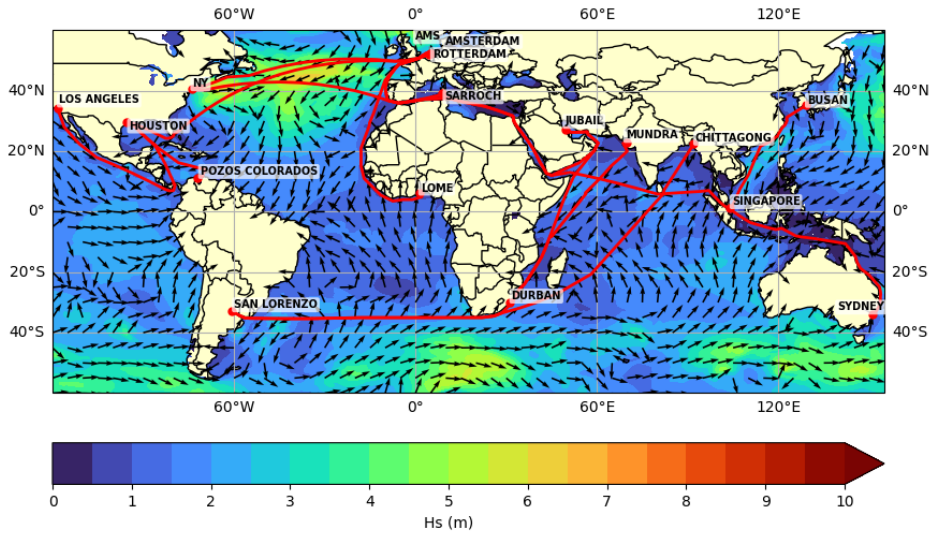

Figure 4.21: Routes for the optimisation plotted together with the weather representing winter (Northern hemisphere).

Table 4.2: Average speed cap, average required energy, average relative added resistance ($R_{\mathrm{AW}}/R_{\mathrm{calm}}$), and number of failed ships for selected routes in summer and winter.

Route	**Avg. speed cap [kn]**		**Avg. req. Energy [MWh]**		**Avg $R_{\mathrm{AW}}/R_{\mathrm{calm}}$ [%]**		**Failed ships**	
	Summer	Winter	Summer	Winter	Summer	Winter	Summer	Winter
Amsterdam - New York	12.00	12.68	1206.82	1465.16	4.00	21.41	0	0
Amsterdam - Lome	12.00	12.09	1499.11	1553.09	5.95	14.01	0	0
Sarroch - New York	12.00	15.68	1435.99	2200.43	5.97	50.47	0	171
Houston - Amsterdam	12.00	15.75	1697.99	2916.34	4.28	42.52	0	201
Houston - Pozos Colorados	12.00	12.00	721.86	774.16	4.72	9.89	0	0
Houston - Los Angeles	12.00	12.00	1601.15	1675.15	3.52	7.05	0	0
San Lorenzo - Mundra	12.00	12.03	3065.73	3285.94	10.38	10.30	0	0
San Lorenzo - Chittagong	12.00	12.03	3308.49	3546.88	10.26	10.88	0	0
Jubail - Rotterdam	12.04	12.00	2447.67	2222.43	3.69	3.49	0	0
Jubail - Durban	12.22	12.00	1818.58	1334.01	19.45	3.64	0	0
Singapore - Sydney	12.00	12.01	1591.77	1415.53	5.64	5.23	0	0
Busan - Singapore	12.00	12.00	958.63	848.69	3.96	5.40	0	0
Singapore - Amsterdam	12.11	12.00	3338.99	2857.47	9.62	5.01	0	0

4.4 Hull optimisation

This section presents the result of unique hulls, more precisely, the 10 best performing and 10 worst performing designs for summer and winter, respectively, and then the summarised result according to the weighting procedure previously described in Section 3.6.6. Performance values in terms of energy are normalised by displacement. The reference IMOIIMAX vessel does not have the same displacement as the new designs it is compared to. It should be noted that, even if the reference vessel has poor performance concerning this measure, it does not mean that it is a bad design. It is a result of the larger vessels having lower resistance per unit volume. This is because the wetted surface is theoretically increased quadratically with the scale factor, but the displacement is increased cubically.

4.4.1 Summer day

For the summer day, all weighted results generated what is presented in Table 4.5. The model indicates that the best design has potential energy savings of 7.9%.

The trend indicates that narrower but deeper hulls have better performance. The length of the ship does not show a clear trend. The top 10 includes designs both close to the lower limit of 170 m and the upper limit of 190 m. The same can be seen for the bottom 10, with a spread of L_{pp} over a large portion of the range. Fig. 4.22 presents the best and worst designs in the 3D sample space previously shown. Excluding the one red dot in the green cluster, it is clear that the model has a consistent prediction, and the trend is confirmed. A purely random distribution would indicate that the model is not reliable.

4.4.2 Winter day

For the winter weather, all weighted results generated what is presented in Table 4.5. The model indicates that the best design has potential energy savings of 8.3%.

The winter day featuring significantly more severe weather conditions than the summer day still has relative results that are similar to the summer day. Here, the best design, again hull number 1, is predicted to save 8.3% of fuel. This increase in savings indicates that in more severe conditions, the potential savings are even greater with this design. The top 4 is exactly the same order as previously, but the rest of the top 10 is slightly changed, with both changed order and some new designs present on the top 10. The trend is, however, still the same, where narrow and deep hulls are indicated to be beneficial. Looking at the average values of the top 10 design, it is a very weak indication that for winter, slightly longer, narrower, and more shallow designs are preferred.

Fig. 4.23 presents the best and worst designs in the 3D sample space previously shown. Excluding the one red dot in the green cluster, it is clear that the model has a consistent prediction, and the trend is confirmed.

Table 4.3: Top 10 and bottom 10 performing hulls for summer weather, ranked by normalised energy consumption.

Rank	Hull #	Lpp [m]	B [m]	T [m]	Rel. Energy Change [%]
1	1	176.3	31.0	12.8	-7.9
2	21	174.3	31.3	12.9	-7.9
3	198	171.7	31.4	12.9	-7.8
4	107	172.0	31.6	12.9	-7.8
5	71	173.6	32.1	12.8	-7.4
6	14	185.6	31.1	12.7	-7.4
7	56	179.9	31.1	12.4	-7.3
8	127	183.1	31.4	12.9	-7.3
9	93	184.1	31.4	12.7	-7.2
10	164	187.2	31.1	12.7	-7.2
Top 10 average		178.8	31.4	12.8	-7.5
...					
192	175	186.8	31.7	10.9	-1.6
193	104	172.6	32.5	11.5	-1.6
194	138	181.5	33.5	10.8	-1.5
195	144	180.1	33.1	10.9	-1.1
196	186	184.1	33.7	10.6	-1.1
197	174	184.0	33.5	10.6	-0.8
198	197	185.1	33.2	10.6	-0.8
199	189	184.2	33.4	10.6	-0.7
200	0	179.0	32.26	11.0	0.0
201	27	184.7	34.0	10.3	+1.1

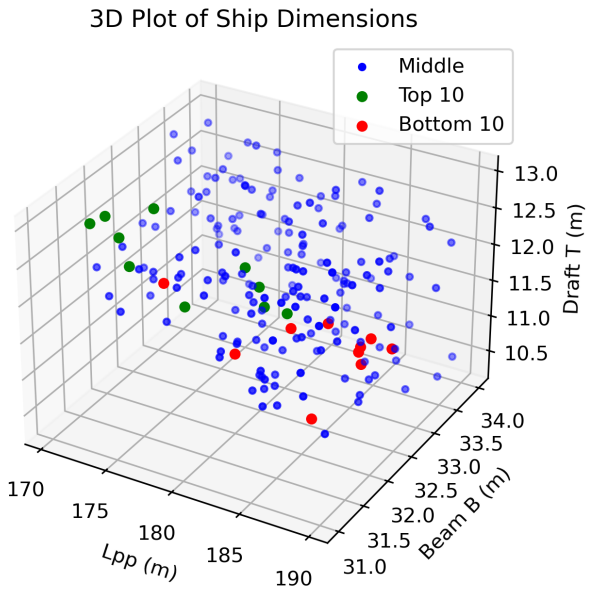

Figure 4.22: All evaluated samples plotted in the 3D domain for the summer weather. The top 10 designs are plotted in green, and the bottom 10 are plotted in red.

Table 4.4: Top 10 and bottom 10 performing hulls for winter weather, ranked by normalised energy consumption.

Rank	Hull #	Lpp [m]	B [m]	T [m]	Rel. Energy Change [%]
1	1	176.3	31.0	12.8	-8.3
2	21	174.3	31.3	12.9	-8.2
3	198	171.7	31.4	12.9	-8.1
4	107	172.0	31.6	12.9	-8.0
5	14	185.6	31.1	12.7	-7.9
6	164	187.2	31.1	12.7	-7.8
7	127	183.1	31.4	12.9	-7.8
8	93	184.1	31.4	12.7	-7.8
9	56	179.9	31.1	12.4	-7.7
10	85	186.2	31.1	12.3	-7.7
Top 10 average		180.0	31.3	12.7	-7.9
...					
192	155	182.4	31.9	11.1	-2.8
193	138	181.5	33.5	10.8	-2.5
194	104	172.6	32.5	11.5	-2.5
195	186	184.1	33.7	10.6	-2.2
196	144	180.1	33.1	10.9	-2.2
197	197	185.1	33.2	10.6	-1.9
198	174	184.0	33.5	10.6	-1.9
199	189	184.2	33.4	10.6	-1.9
200	27	184.7	34.0	10.3	0.0
201	0	179.0	32.26	11.0	0.0

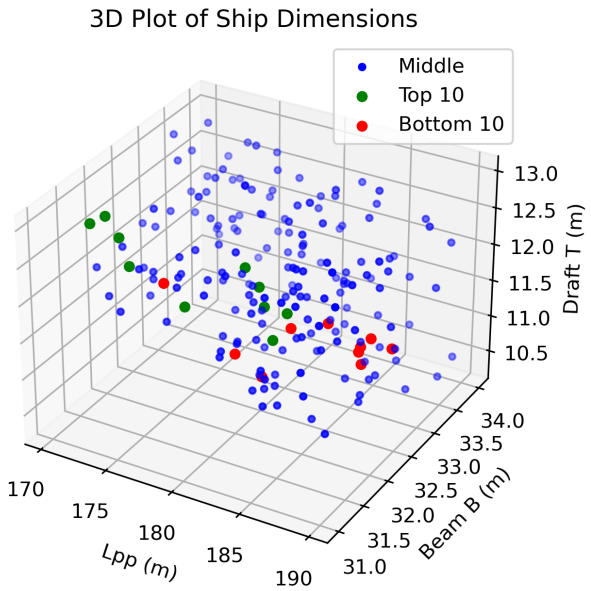

Figure 4.23: All evaluated samples plotted in the 3D domain for the winter weather. The top 10 designs are plotted in green, and the bottom 10 are plotted in red.

4.4.3 Average of winter and summer

The overall best design is found by averaging all performance-demanding measures between winter and summer results, as explained in Section 3.6.6. The results are presented in Table 4.5, ranked by the displacement normalised energy consumption. All samples with highlighting of the top 10 and bottom 10 are again presented in the 3D domain in Fig. 4.24. Since the trend was similar in both winter and summer separately, the same trend is seen for the average of both seasons. The best hull is design number 1, with estimated fuel savings of 8.1% compared to the IMOIIMAX vessels. The fact that the first sample has the best performance is purely random.

Table 4.5: Top 10 and bottom 10 performing hulls ranked by normalised energy consumption.

Rank	**Hull #**	**Lpp [m]**	**B [m]**	**T [m]**	**Rel. Energy Change [%]**
0	1	176.3	31.0	12.8	-8.1
1	21	174.3	31.3	12.9	-8.0
2	198	171.7	31.4	12.9	-7.9
3	107	172.0	31.6	12.9	-7.9
4	14	185.6	31.1	12.7	-7.6
5	127	183.1	31.4	12.9	-7.6
6	56	179.9	31.1	12.4	-7.5
7	71	173.6	32.1	12.8	-7.5
8	164	187.2	31.1	12.7	-7.5
9	93	184.1	31.4	12.7	-7.5
Top 10 average		178.8	31.3	12.8	-7.7
...					
192	175	186.8	31.7	10.9	-2.2
193	104	172.6	32.5	11.5	-2.0
194	138	181.5	33.5	10.8	-2.0
195	144	180.1	33.1	10.9	-1.6
196	186	184.1	33.7	10.6	-1.6
197	174	184.0	33.5	10.6	-1.3
198	197	185.1	33.2	10.6	-1.3
199	189	184.2	33.4	10.6	-1.3
200	0	179.0	32.26	11.0	0.0
201	27	184.7	34.0	10.3	+0.6

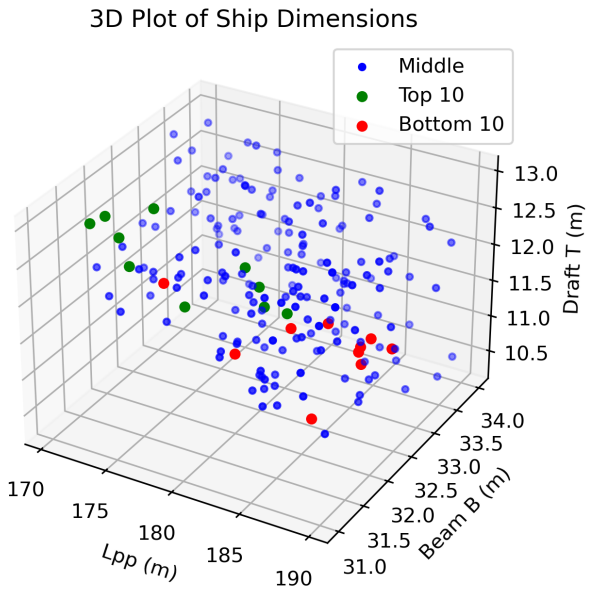

Figure 4.24: All evaluated samples plotted in the 3D domain for the average of summer and winter weather. The top 10 designs are plotted in green and the bottom 10 are plotted in red.

4.4.4 Detailed analysis of optimum hull design

The optimum hull has the main dimensions shown in Table 4.6.

Table 4.6: Comparison of reference and best design. All energy and resistance values are normalised by displacement.

	Reference hull	**Best design**
Lpp	179	183
B	32.26	31
T	11	12.8
C_B	0.78	0.79
$\Delta R_{AW}[N/m^3]$	-	-13.7%
$\Delta P_d^{calm}[kW/m^3]$ at design speed	-	-8.2%
$\Delta Energy$	-	-8.1%
Avg Speed Cap [kn]	12.29	12.32
Max speed cap [kn]	13.97	13.97
Houston - Amsterdam avg speed [kn]	11.41	11.37

We see that the energy saved is less than the reduction of calm water resistance and added resistance in waves. This is due to the new designs having slightly different displacements but operating with the same machinery, meaning that the total resistance is higher in absolute numbers and resulting in more speed loss. Forcing the ship to compensate with higher speeds in other parts of the route, where possible. The higher speed negatively affects the energy consumption.

5

Discussion

This chapter presents the authors' subjective opinions and ideas regarding the content of previous chapters. Both the literature review, method, and result feature aspects and assumptions that have a large influence on the result.

5.1 SNNM

The SNNM model has been an important part of this methodology, and several aspects of both the initial and improved models are up for discussion.

5.1.1 Initial Formula

The SNNM method should be a transparent and efficient tool to implement by shipowners, researchers, and other actors and stakeholders within the marine industry. The method has proven to be complex, with many levels of "if statements" and extensive equations. Moreover, the inconsistencies between different versions without proper comments and motivations for changes make the method very non-transparent. This makes it more difficult for shipowners, such as Stena, to implement their own scripts and instead might need to outsource these services.

5.1.2 Improved model

The improved model has very promising results when comparing it to the measurement data. However, as mentioned, when the correction is in the same order of magnitude as the initial value given by the SNNM method, something is not right. The authors suggest that the resistance prediction must be made more accurate before the improved model is mature and ready to use. It is necessary, when training the model, to ensure that what is left from the resistance given by the measured data is, in fact, added resistance in waves and not something else. The biofouling resistance, which according to what is described in Section 2.1.4, has a significant impact on the total resistance of the ship. Trying to make the model correct for this with the input variables used for added resistance in waves is wrong and might produce unexpected results when extrapolating to other hull designs, which is exactly what this thesis is doing.

5.2 Data Volume

The data supplied by Stena contained eight months of measurements, with part of the data filtered out due to port stays. In machine learning and linear regression, more data is always better, as long as the quality of the data is kept constant. With only eight months of data, there is a significant risk of creating a bias towards the specific conditions encountered. The accuracy of the model will not be as good when extrapolating to new conditions.

The data should ideally include as wide a range of conditions and locations as possible in order to create a good model. It would also be beneficial to include data from a range of ships, preferably different sizes as well, to be able to use the machine learning calibration model on new hull designs and to utilise it in the optimisation loop.

5.3 Routing tool

The routing tool used is based on `marnet_geograph` function from `scgraph` in Python (Makowski 2023). This is an open-source, publicly available tool. The tool does not consider traffic separation schemes or shallow areas. Thus, it will often keep very close to the coast to minimise distance when rounding a cape. See an example of the Cape of Good Hope. This influences the encountered weather and waves. Thus, not give a proper representation of what would be encountered in real life

Another limitation in this tool is the waypoint density. If there are few limitations to the routing and the route can be straight, the distance between waypoints can be very large, up to a day or more. This leads to lower resolution in the calculation, and changes in weather along this straight line will be neglected.

5.4 Accuracy of the predictions

The accuracy of the predicted performance values is not quantified in this thesis; however, one could subjectively discuss the accuracy. First and foremost, the SNNM model has its drawbacks, especially in oblique and following seas. It is also mainly intended for sea states that are above the very low threshold of what is considered calm seas speed trials. The severe weather encountered in this optimisation study might be well outside its range with sufficient accuracy. Moreover, the performance values regarding fuel saving is not to be taken as an absolute truth, but more an indication. It is, however, deemed that the trends are correct. As mentioned in Section 4.2.1, there is potentially other types of resistance captured in the extraction of the added resistance in waves of the measurement data, which makes the comparison unreliable and also contributes to the regression of the calibration model, capturing other aspects than only the added resistance in waves.

6

Conclusion

This thesis set out to optimise the main dimensions of next-generation MR tankers by developing a performance assessment methodology based on real trading routes and hindcast weather data. The focus was on evaluating added resistance in waves using the SNNM method and investigating the potential for improving model accuracy through machine learning corrections based on full-scale measurements from existing IMOIIMAX vessels.

A flexible performance model framework was developed and delivered to Stena Teknik, enabling both analysis of recorded operational data and evaluation or optimisation of new hull main dimensions.

In this thesis, eight months of full-scale data from Stena Immortal, was used for a machine learning correction that significantly improved prediction accuracy for added resistance in waves, from a R^2 value of 0.148 with the standard SNNM method to 0.910 after correction. This demonstrates the potential of using operational data to improve the resistance prediction on an existing ship.

The improved model generated promising results when comparing the correlation of measured and predicted R_{AW}; however, the model is deemed not mature enough to be used for extrapolation and implementation on new designs. Further tuning of the model is needed, and the full scale data needs to be more thoroughly investigated. The predicted power is simply not accurate enough to be able to use full scale data to tune the SNNM model without running into unwanted effects.

Despite these limitations, the optimization results suggest that a narrower and deeper hull form could reduce fuel consumption by up to 8%, under the assumption that the performance model is accurate. While added resistance in waves contributes to performance differences between designs, the results indicate that calm water resistance remains the dominant factor in overall fuel efficiency.

The proposed methodology offers a structured approach for early-stage design exploration and decision support at Stena Teknik. Future work should focus on refining the full-scale data processing, improving model reliability for extrapolation. With further development, this tool could support the identification of optimal hull forms tailored to real operational profiles and environmental conditions.

7

Future Work

This master thesis has accomplished a lot and covered many areas. The tool however, is not completely ready to be used as a reliable decision-making tool. Some assumptions need to be addressed, but the authors also present potential applications that this tool can be extended and cover.

7.1 Larger set of weather conditions

One very relevant area to continue work on is to include a larger set of weather conditions. Preferably, many years and as many time instances as possible. This is needed to get a true representation of the environmental conditions and remove the probability aspect of the statistics. When this is implemented and not every weather can be checked. Some form of weather routing needs to be implemented such that the routes are avoiding the most severe storms, just as in reality.

7.2 Improving the model

The tool developed and models implemented can, of course, be improved. One way to improve the tool is to implement a model for biofouling growth and corresponding resistance increase. This will increase the accuracy of the standard model and also the improved model.

Other ways to improve the tool is to run the linear regression on a larger data set, as discussed in Section 5.2.

7.3 Streamline the code

The code today is computationally heavy and could be made more efficient such that it runs faster. A thorough investigation should be made to find parts of the code that are bottlenecking the performance. Right now, the most computationally heavy part is the 2D integration of the directional spectrum. Here, one could reduce the number of discretisation points or implement a more efficient calculation method. The area of integration that was chosen early in the project is also larger than necessary; the range of wave frequency, $0.01 < \omega < 6$, equivalent to $\lambda_{max} \approx 617km$, could be

reduced. There is potential to save a lot of computational time here. According to Gerritsma and Beukelman (1972), the choice of wave length should be around $0.5 < \sqrt{L/\lambda} < 1.6$, which in this case would give a wave length of $\sim 700 > \lambda > 70$ meters, this is however for motion induced resistance, we also include wave reflection resistance thus we would need shorter wave lengths as well.

To take advantage of Python's libraries NumPy and Pandas, the code could be rewritten to handle vectorisation, which would reduce the computational time significantly, if possible.

7.4 Implement potential applications

The development of a tool to access, process and map weather data to voyage data to assess local weather conditions regarding wave and wind environment. This can be implemented for evaluating weather routing tools or assessing the performance of wind-assisted ships in a case study type of project.

Since the format of the data for the hindcast is the same as the forecast, there is a huge potential to use it for actual weather routing tools to avoid areas with unfavourable wave conditions and try to exploit favourable conditions for wind-assisted propulsion.

Bibliography

Boom, Henk van den, Hans Huisman, and Frits Mennen. 2019. "New Guidelines for Speed/Power Trials Level playing field established for IMO EEDI" (October).

Breiman, L. 2001. "Random forests" [in English]. *MACHINE LEARNING* (VAN GODEWIJCKSTRAAT 30, 3311 GZ DORDRECHT, NETHERLANDS) 45, no. 1 (October): 5–32. ISSN: 0885-6125. https://doi.org/10.1023/A:1010933404324.

Chatterjee, Samprit, and Ali S. Hadi. 2012. *Regression Analysis by Example.* Wiley. https://sadbhavnapublications.org/research-enrichment-material/2-Statistical-Books/Regression-Analysis-by-Example.pdf.

Chen, Tianqi, and Carlos Guestrin. 2016. "XGBoost: A Scalable Tree Boosting System." In *Proceedings of the 22nd ACM SIGKDD International Conference on Knowledge Discovery and Data Mining,* 785–794. KDD '16. San Francisco, California, USA: Association for Computing Machinery. ISBN: 9781450342322. https://doi.org/10.1145/2939672.2939785. https://doi.org/10.1145/2939672.2939785.

Climate Data Store. 2025. "Background." (Accessed: 2025-02-28). https://cds.climate.copernicus.eu/background.

Copernicus Marine Services. 2025a. "Copernicus Marine Service." (Accessed: 2025-02-28). https://marine.copernicus.eu/about.

Copernicus Marine Services. 2025b. "Global Ocean Physics Analysis and Forecast." (Accessed: 2025-02-28). https://doi.org/10.48670/moi-00016.

Faltinsen, Odd M., Knut J. Minsaas, Nicolas Liapis, and Svein O. Skjördal. 1980. "Prediction of Resistance and Propulsion of a Ship in a Seaway." *Proceedings of the 13th Symposium on Naval Hydrodynamics.*

Fujimoto, Wataru, Kinya Ishibashi, and Tingyao Zhu. 2024. "Analyzing AIS and wave hindcast data for global wave scatter diagrams with seasonality." *Ocean Engineering* 314:119647. ISSN: 0029-8018. https://doi.org/https://doi.org/10.1016/j.oceaneng.2024.119647. https://www.sciencedirect.com/science/article/pii/S0029801824029858.

Gerritsma, Prof.Ir. J., and W. Beukelman. 1972. "Analysis of the resistance increase in waves of a fast cargo ship." *International Shipbuilding Progress* 19 (217): 285–293. https://doi.org/10.3233/ISP-1972-1921701. eprint: https://doi.org/10.3233/ISP-1972-1921701. https://doi.org/10.3233/ISP-1972-1921701.

Havelock, T.H. 1942. "XLVII. The drifting force on a ship among waves." *The London, Edinburgh, and Dublin Philosophical Magazine and Journal of Science* 33 (221): 467–475. https://doi.org/10.1080/14786444208521213. eprint: https://doi.org/10.1080/14786444208521213. https://doi.org/10.1080/14786444208521213.

Hersbach, Hans, Bill Bell, Paul Berrisford, Shoji Hirahara, András Horányi, Joaquín Muñoz-Sabater, Julien Nicolas, et al. 2020. "The ERA5 global reanalysis." *Quarterly Journal of the Royal Meteorological Society* 146 (730): 1999–2049. https://doi.org/https://doi.org/10.1002/qj.3803. eprint: https://rmets.onlinelibrary.wiley.com/doi/pdf/10.1002/qj.3803. https://rmets.onlinelibrary.wiley.com/doi/abs/10.1002/qj.3803.

Hogben, N. 1988. *Global wave statistics.* British Maritime Technology Limited.

Holtrop, J., and G.G.J. Mennen. 1982. "An approximate power prediction method." *International Shipbuilding Progress* 29 (July): 166–170. https://doi.org/10.3233/ISP-1982-2933501.

IMO. 2025a. "IMO's work to cut GHG emissions from ships." (Accessed: 2025-05-27). https://www.imo.org/en/MediaCentre/HotTopics/Pages/Cutting-GHG-emissions.aspx.

IMO. 2025b. "Improving the energy efficiency of ships." (Accessed: 2025-05-27). https://www.imo.org/en/OurWork/Environment/Pages/Improving%20the%20energy%20efficiency%20of%20ships.aspx.

ITTC. 2002. *The Specialist Committee on Waves: Final Report and Recommendations to the 23rd ITTC.*

ITTC. 2014. *ITTC - Recommended Procedures and Guidelines: Procedure, Preparation, Conduct and Analysis of Speed/Power Trials 7.5-04-01-01.2.*

ITTC. 2021. *ITTC - Recommended Procedures and Guidelines: Procedure, Preparation, Conduct and Analysis of Speed/Power Trials 7.5-04-01-01.1.*

ITTC. 2022. *ITTC - Recommended Procedures and Guidelines: Procedure, Preparation, Conduct and Analysis of Speed/Power Trials 7.5-04-01-01.1.*

ITTC. 2024. *ITTC - Recommended Procedures and Guidelines: Procedure, Preparation, Conduct and Analysis of Speed/Power Trials 7.5-04-01-01.1.*

Janssen, Peter A.E.M., and Jean-Raymond Bidlot. 2018. "Progress in Operational Wave Forecasting." IUTAM Symposium on Wind Waves, *Procedia IUTAM* 26:14–29. ISSN: 2210-9838. https://doi.org/https://doi.org/10.1016/j.piutam.2018.03.003. https://www.sciencedirect.com/science/article/pii/S2210983818300038.

Jinkine, V., and V. Ferdinande. 1974. "A method for predicting the added resistance of fast cargo ships in head waves." *International Shipbuilding Progress* 21 (238): 149–167. https://doi.org/10.3233/ISP-1974-2123801. eprint: https://doi.org/10.3233/ISP-1974-2123801. https://doi.org/10.3233/ISP-1974-2123801.

Krogstad, Harald, and Øivind Arntsen. 2000. *Linear Wave Theory Part B.* Norwegian university of science / technology.

Lang, Xiao, and Wengang Mao. 2021. "A Practical Speed Loss Prediction Model at Arbitrary Wave Heading for Ship Voyage Optimization." *Journal of Marine Science and Application* 20 (August). https://doi.org/10.1007/s11804-021-00224-z.

Lang, Xiao, Da Wu, and Wengang Mao. 2022. "Comparison of supervised machine learning methods to predict ship propulsion power at sea." *Ocean Engineering* 245:110387. ISSN: 0029-8018. https://doi.org/https://doi.org/10.1016/j.oceaneng.2021.110387. https://www.sciencedirect.com/science/article/pii/S0029801821016802.

Larsson, Lars, and Hoyte C. Raven. 2010. *Principles of Naval Architecture Series - Ship Resistance and Flow.* Society of Naval Architects / Marine Engineers (SNAME). ISBN: 978-0-939773-76-3. https://app.knovel.com/hotlink/toc/id:kpPNASSRF2/principles-naval-architecture-7/principles-naval-architecture-7.

Lewis, Edward V. 1989. *Principles of naval Architecture Second Revision.* The Society of Naval Architects / Marine Engineers.

Liu, Shukui, and Apostolos Papanikolaou. 2016. "Fast approach to the estimation of the added resistance of ships in head waves." *Ocean Engineering* 112:211–225. ISSN: 0029-8018. https://doi.org/https://doi.org/10.1016/j.oceaneng.2015.12.022. https://www.sciencedirect.com/science/article/pii/S0029801815006769.

Liu, Shukui, and Apostolos Papanikolaou. 2020. "Regression analysis of experimental data for added resistance in waves of arbitrary heading and development of a semi-empirical formula." *Ocean Engineering* 206:107357. ISSN: 0029-8018. https://doi.org/https://doi.org/10.1016/j.oceaneng.2020.107357. https://www.sciencedirect.com/science/article/pii/S0029801820303887.

Liu, Shukui, Apostolos Papanikolaou, and George Zaraphonitis. 2015. "Practical approach to the added resistance of a ship in short waves." June.

Makowski, Connor. 2023. "scgraph." (Accessed 2025-04-10). https://pypi.org/project/scgraph/.

MAN Energy Solutions. 2023. "Basic Principles of ship propulsion." (Accessed 2025-02-27). https://www.man-es.com/docs/default-source/document-sync/basic-principles-of-ship-propulsion-eng.pdf.

Maruo, Prof. Hajime. 1957. "The excess resistance of a ship in rough seas." *International Shipbuilding Progress* 4 (35): 337–345. https://doi.org/10.3233/ISP-1957-43501. eprint: https://doi.org/10.3233/ISP-1957-43501. https://doi.org/10.3233/ISP-1957-43501.

McEntee, William. 1915. "Variation of frictional resistance of ships with condition of wetted surface." *Trans. Soc. Nav. Arch. Mar. Eng.*

Miles, Alistair, jakirkham, Joe Hamman, Dimitri Papadopoulos Orfanos, David Stansby, M Bussonnier, Josh Moore, et al. 2025. *zarr-developers/zarr-python: v3.0.4.* https://doi.org/10.5281/zenodo.14914189.

Olive, David J. 2017. *Linear Regression.* Springer Cham. https://doi.org/https://doi.org/10.1007/978-3-319-55252-1.

Parsons, Michael G. 2003. "Ship Design and Construction, Volumes 1-2." Chap. 11. Society of Naval Architects / Marine Engineers (SNAME).

Pérez Arribas, F. 2007. "Some methods to obtain the added resistance of a ship advancing in waves." *Ocean Engineering* 34 (7): 946–955. ISSN: 0029-8018. https://doi.org/https://doi.org/10.1016/j.oceaneng.2006.06.002. https://www.sciencedirect.com/science/article/pii/S0029801806001818.

S&P Maritime. 2025. "Ship details: STENA IMMORTAL." (Accessed 2025-04-11). https://maritime.ihs.com/Ships/Details/Index/9685475.

Schultz, Michael P. 2007. "Effects of coating roughness and biofouling on ship resistance and powering." *Biofouling* 23 (5): 331–341. https://doi.org/10.1080/08927010701461974. eprint: https://doi.org/10.1080/08927010701461974. https://doi.org/10.1080/08927010701461974.

Schultz, Michael P., and Geoffrey W. Swain. 2000. "The influence of biofilms on skin friction drag." *Biofouling* 15 (1-3): 129–139. https://doi.org/10.1080/08927010009386304. https://www.scopus.com/inward/record.uri?eid=2-s2.0-0033938277&doi=10.1080%2f08927010009386304&partnerID=40&md5=4dbc0a703c5e1d67860997bcba16f6bf.

Song, Soonseok, Yigit Kemal Demirel, and Mehmet Atlar. 2020. "Penalty of hull and propeller fouling on ship self-propulsion performance." *Applied Ocean Research* 94:102006. ISSN: 0141-1187. https://doi.org/https://doi.org/10.1016/j.apor.2019.102006. https://www.sciencedirect.com/science/article/pii/S0141118719305735.

Strom-Tejsen, J, H Yeh, and D Moran. 1973. "Added resistance in waves." *Trans Soc Nav Archit Mar Eng.*

Turan, Osman, Yigit Kemal Demirel, Sandy Day, and Tahsin Tezdogan. 2016. "Experimental Determination of Added Hydrodynamic Resistance Caused by Marine Biofouling on Ships." *Transportation Research Procedia* 14:1649–1658. ISSN: 2352-1465. https://doi.org/https://doi.org/10.1016/j.trpro.2016.05.130. https://www.sciencedirect.com/science/article/pii/S2352146516301314.

Uzun, Dogancan, Yigit Kemal Demirel, Andrea Coraddu, and Osman Turan. 2019. "Time-dependent biofouling growth model for predicting the effects of biofouling on ship resistance and powering." *Ocean Engineering* 191:106432. ISSN: 0029-8018. https://doi.org/https://doi.org/10.1016/j.oceaneng.2019.106432. https://www.sciencedirect.com/science/article/pii/S0029801819305803.

Wang, Jinbao, Sebastian Bielicki, Florian Kluwe, Hideo Orihara, Gongzheng Xin, Kenichi Kume, Semyun Oh, Shukui Liu, and Peiyuan Feng. 2021. "Validation study on a new semi-empirical method for the prediction of added resistance in waves of arbitrary heading in analyzing ship speed trial results." *Ocean Engineering* 240:109959. ISSN: 0029-8018. https://doi.org/https://doi.org/10.1016/j.oceaneng.2021.109959. https://www.sciencedirect.com/science/article/pii/S0029801821013020.

Wikipedia. 2025. "Null Island." (Accessed: 2025-05-17). https://en.wikipedia.org/wiki/Null_Island.

WikiWaves. 2025. "Linear." (Accessed: 2025-02-27). https://wikiwaves.org/Linear_Theory_of_Ocean_Surface_Waves.

Woods Hole Oceanographic Institution. 1952. *Marine fouling and its prevention.* united States. Navy Dept. Bureau of Ships.

A

SNNM method as per ITTC 7.5-04-01-01.1

G.3. Semi-empirical method for predicting the added resistance of a ship advancing in waves of arbitrary directions (SNNM)

A Semi-empirical method (Liu S., et Al. 2015) has been developed to approximate the transfer function of the mean resistance increase in regular waves of arbitrary headings.

The mean added resistance in regular waves R_{wave} is calculated as the sum of the motion-induced component R_{AWM} and the wave reflection induced component R_{AWR}.

$$R_{\mathrm{wave}}(\omega,\alpha;V_S) = R_{\mathrm{AWM}} + R_{\mathrm{AWR}} \tag{G-13}$$

The expression of R_{AWM} is given by

$$R_{\mathrm{AWM}} = 3859.2\rho_s g\zeta_A{}^2 \frac{B^2}{L_{\mathrm{PP}}} C_B^{1.34} k_{yy}{}^2 \cdot a_1 a_2 a_3 \bar{\omega}^{b_1} e^{\frac{b_1}{d_1}(1-\bar{\omega}^{d_1})} \tag{G-14}$$

where

$$\bar{\omega} = 2.142\sqrt[3]{k_{yy}}\sqrt{\frac{L_{\mathrm{pp}}}{2\pi g}}\left(\frac{C_B}{0.65}\right)^{0.17} \cdot \left[1 - \frac{0.111}{C_B}\left(\ln\frac{B}{T_{\mathrm{deep}}} - \ln 2.75\right)\right] \cdot \left[\left(-1.377Fr^2 + 1.157Fr\right)|\cos\alpha| + \frac{0.618(13+\cos 2\alpha)}{14}\right]\omega \tag{G-15}$$

$$a_1\left(0 \le \alpha \le \frac{\pi}{2}\right) = \left(\frac{0.87}{C_B}\right)^{(1+Fr)\cos\alpha}\left(\ln\frac{B}{T_{\mathrm{deep}}}\right)^{-1}\frac{(1+2\cos\alpha)}{3} \tag{G-16}$$

$$a_1(\alpha=\pi) = \begin{cases}\left(\frac{0.87}{C_B}\right)^{1+Fr_{\mathrm{rel}}}\left(\ln\frac{B}{T_{\mathrm{deep}}}\right)^{-1} & V_S > V_g \text{ and } Fr_{\mathrm{rel}} \ge 0.12\\ \left(\frac{0.87}{C_B}\right)\left(\ln\frac{B}{T_{\mathrm{deep}}}\right)^{-1} & \text{elsewhere}\end{cases} \tag{G-17}$$

$$a_2\left(0 \le \alpha \le \frac{\pi}{2}\right) = \begin{cases}0.0072 + 0.1676Fr & \text{for } Fr < 0.12\\ Fr^{1.5}e^{-3.5Fr} & \text{for } Fr \ge 0.12\end{cases} \tag{G-18}$$

$$a_2(\alpha=\pi) = \begin{cases}0.0072\left(2V_S/V_g - 1\right) & \text{for } V_S \le V_g\\ 0.0072 + 0.1676Fr_{\mathrm{rel}} & \text{for } V_S > V_g \text{ and } Fr_{\mathrm{rel}} < 0.12\\ Fr_{\mathrm{rel}}{}^{1.5}e^{-3.5Fr_{\mathrm{rel}}} & \text{for } V_S > V_g \text{ and } Fr_{\mathrm{rel}} \ge 0.12\end{cases} \tag{G-19}$$

$$a_3 = 1.0 + 28.7\mathrm{atan}\frac{|T_A - T_F|}{L_{\mathrm{PP}}} \tag{G-20}$$

$$b_1 = \begin{cases}11.0 & \text{for } \bar{\omega} < 1\\ -8.5 & \text{elsewhere}\end{cases} \tag{G-21}$$

$$d_1 = \begin{cases} 566\left(\frac{L_{PP}C_B}{B}\right)^{-2.66} & \text{for } \bar{\omega} < 1 \\ -566\left(\frac{L_{PP}}{B}\right)^{-2.66}(4 - 125\text{atan}\frac{|T_A - T_F|}{L_{PP}}) & \text{elsewhere} \end{cases} \quad \text{(G-22)}$$

R_{AWM} in stern oblique waves, i.e. for $\frac{\pi}{2} \leq \alpha \leq \pi$, is found by linear interpolation between the values in beam and following waves.

The expression of the added resistance due to reflection effect, R_{AWR}, takes the following form:

$$R_{AWR} = \sum_{i=1}^{4} R_{AWR,i} \quad \text{(G-23)}$$

where

$$R_{AWR,1} = = \frac{2.25}{4}\rho_s g B \zeta_A{}^2 \alpha_{T^*}\left\{\sin^2(E_1+\alpha) + \frac{2\omega V_S}{g}[\cos\alpha - \cos E_1 \cos(E_1+\alpha)]\right\}\left(\frac{0.87}{C_B}\right)^{(1+4\sqrt{Fr})f(\alpha)}$$

for $0 \leq \alpha \leq \pi - E_1$ (G-24)

$$R_{AWR,2} = = \frac{2.25}{4}\rho_s g B \zeta_A{}^2 \alpha_{T^*}\left\{\sin^2(E_1-\alpha) + \frac{2\omega V_S}{g}[\cos\alpha - \cos E_1 \cos(E_1-\alpha)]\right\}\left(\frac{0.87}{C_B}\right)^{(1+4\sqrt{Fr})f(\alpha)}$$

for $0 \leq \alpha \leq E_1$ (G-25)

$$R_{AWR,3} = -\frac{2.25}{4}\rho_s g B \zeta_A{}^2 \alpha_{T^*}\left\{\sin^2(E_2-\alpha) + \frac{2\omega V_S}{g}[\cos\alpha - \cos E_2 \cos(E_2-\alpha)]\right\}$$

for $E_2 \leq \alpha \leq \pi$ (G-26)

$$R_{AWR,4} = -\frac{2.25}{4}\rho_s g B \zeta_A{}^2 \alpha_{T^*}\left\{\sin^2(E_2+\alpha) + \frac{2\omega V_S}{g}[\cos\alpha - \cos E_2 \cos(E_2+\alpha)]\right\}$$

for $\pi - E_2 \leq \alpha \leq \pi$ (G-27)

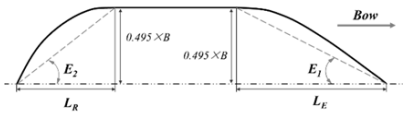

Figure G-3. Sketch of the half waterline of a ship and related definitions

$$f(\alpha) = \begin{cases} \cos\alpha & 0 \leq \alpha \leq E_1 \\ 0 & \alpha > E_1 \end{cases} \quad \text{(G-28)}$$

α_{T^*} is the draft coefficient, calculated as:

$$\alpha_{T^*} = \begin{cases} 1 - e^{-4\pi\left(\frac{T^*}{2\pi g/\omega^2} - \frac{T^*}{2.5L_{\mathrm{pp}}}\right)} & \frac{2\pi g}{\omega^2 L_{\mathrm{pp}}} \leq 2.5 \\ 0 & \frac{2\pi g}{\omega^2 L_{\mathrm{pp}}} > 2.5 \end{cases} \quad \text{(G-29)}$$

where for $R_{\mathrm{AWR},1}$ and $R_{\mathrm{AWR},2}$

$$T^* = T_{\mathrm{deep}} \quad \text{(G-30)}$$

and for $R_{\mathrm{AWR},3}$ and $R_{\mathrm{AWR},4}$

$$T^* = \begin{cases} T_{\mathrm{deep}}\left(4 + \sqrt{|\cos\alpha|}\right)/5 & C_{\mathrm{B}} \leq 0.75 \\ T_{\mathrm{deep}}\left(2 + \sqrt{|\cos\alpha|}\right)/3 & C_{\mathrm{B}} > 0.75 \end{cases} \quad \text{(G-31)}$$

where

L_{PP}: is the ship length between perpendiculars in meters;
B: is the ship's breadth in meters;
T: is the wave period in seconds;
T_{M}: is the draught at midships in meters;
T_{F}: is the draught at the forward perpendicular in meters;
T_{A}: is the draught at aft perpendicular in meters;
T_{deep} = max (T_{F}, T_{A});
L_{E}: is the length of entrance of the waterline in meters, shown in Fig G 3;
E_1: is the angle of entrance on the waterline in radians, as shown in Figure G-3;
L_{R}: is the length of run of the waterline in meters, shown in Fig G3;
E_2: is the angle of the run on the waterline in radians, as shown in Figure G-3;
C_{B}: is the block coefficient;
k_{yy}: is the ratio of radius of gyration of pitch and L_{PP};
Fr: is the Froude Number, $Fr = V_{\mathrm{S}}/\sqrt{gL_{\mathrm{PP}}}$;
$Fr_{\mathrm{rel}} = \left(V_{\mathrm{S}} - V_{\mathrm{g}}\right)/\sqrt{gL_{\mathrm{PP}}}$;
V_{g} is the group velocity of the incident wave, $V_{\mathrm{g}} = \frac{g}{2\omega}$;
V_{S} is the ship's speed through the water in meters per second;
α: is the angle between ship's heading and wave direction relative to the bow in radians; 0 means head waves;
ζ_{A}: is the wave amplitude in meters;
ω: is the circular frequency of regular component waves in radians per second.

With the following restrictions:

- 75 m ≤ L_{PP} ≤ 400 m;
- 5.0 ≤ L_{PP}/B ≤ 8.0;
- 2.0 ≤ B/T ≤ 8.0;
- 0.52 ≤ C_{B} ≤ 0.88;
- 0.09 ≤ Fr ≤ 0.30.

the method is applicable to the mean resistance increase in short crested irregular waves R_{AW}, according to formula (G.32).

$$R_{\mathrm{AW}} = 2\int_0^{2\pi}\int_0^{\infty} \frac{R_{\mathrm{wave}}(\omega,\alpha;V_{\mathrm{S}})}{{\zeta_{\mathrm{A}}}^2} E(\omega,\alpha)\,d\omega\,d\alpha \quad \text{(G-32)}$$

where

E: is the directional wave spectrum. (see eq. 10)

DEPARTMENT OF MECHANICS AND MARITIME SCIENCES
CHALMERS UNIVERSITY OF TECHNOLOGY
Gothenburg, Sweden
www.chalmers.se

CHALMERS
UNIVERSITY OF TECHNOLOGY